



## **Investigation of water softening using ceramic adsorbents in a continuous adsorption process**

Downloaded from: <https://research.chalmers.se>, 2026-05-11 09:32 UTC

Citation for the original published paper (version of record):

Danesh, E., Abbasi, M., Noroozi Chegeni, M. et al (2026). Investigation of water softening using ceramic adsorbents in a continuous adsorption process. *Scientific Reports*, 16(1).

<http://dx.doi.org/10.1038/s41598-026-38953-2>

N.B. When citing this work, cite the original published paper.



## OPEN Investigation of water softening using ceramic adsorbents in a continuous adsorption process

Elnaz Danesh<sup>1</sup>, Mohsen Abbasi<sup>1</sup>✉, MohammadMahdi Noroozi<sup>2</sup>, Masoud Mofarehi<sup>1</sup>, Ali Izadbakhsh<sup>1</sup> & Mohammad Akrami<sup>3</sup>

Ceramic adsorbents offer a sustainable and cost-effective approach to water treatment, particularly for reducing water hardness. This study aimed to evaluate the performance of natural zeolite and activated alumina, modified with NaNO<sub>3</sub> and H<sub>2</sub>SO<sub>4</sub>, respectively, in a continuous fixed-bed column system for water softening. Adsorption experiments were conducted under varying operational conditions, including column diameters (1 and 1.5 cm), flow rates (10 and 20 mL/min), and an operation time of 600 min. The optimal setup, 1.5 cm column diameter and 10 mL/min flow rate, yielded bed saturation times of 600 min for modified zeolite and 570 min for modified alumina. NaNO<sub>3</sub>-modified zeolite achieved removal efficiencies of 99.23% for total hardness, 99.37% for calcium, and 99.17% for magnesium. Breakthrough and saturation times indicated superior performance compared to unmodified adsorbents. Kinetic models, including Thomas, Adams–Bohart, and Yoon–Nelson, were applied, with the Thomas and Yoon–Nelson models fitting best ( $R^2 \approx 0.98$ ). The findings demonstrate that surface modification enhances the adsorption capacity of ceramic materials, highlighting their potential for efficient and scalable water hardness treatment in continuous systems.

**Keywords** Water treatment, Adsorbent, Water hardness, Natural zeolite, Activated alumina, Breakthrough curve

Ensuring safe drinking water is essential for public health and human quality of life<sup>1,2</sup>. Among various water contaminants, water hardness, primarily caused by multivalent metal ions, especially calcium (Ca<sup>2+</sup>) and magnesium (Mg<sup>2+</sup>), is a significant concern<sup>3</sup>. Excessive calcium and magnesium levels in drinking water have been linked to various health issues, such as osteoporosis, kidney stones, colon cancer, and hypertension<sup>4</sup>. The World Health Organization (WHO) recommends permissible levels of 40–80 ppm for calcium and 20–30 ppm for magnesium in drinking water, corresponding to a total hardness of approximately 2–4 mmol/L<sup>3</sup>. Moreover, water hardness causes sedimentation and scaling in water supply infrastructure, reducing water flow, increasing energy consumption, and significantly elevating maintenance costs<sup>5</sup>.

Several methods, including thermal treatment, membrane processes, magnetic methods, ion exchange, and adsorption, have been proposed to mitigate water hardness<sup>6–9</sup>. Among these, adsorption stands out due to its cost-effectiveness, operational simplicity, and flexibility in design<sup>10</sup>. Various materials including activated alumina, activated carbon, biomass, clay, and zeolite, have been explored extensively as adsorbents for hardness removal<sup>11,12</sup>. Natural zeolite, particularly clinoptilolite, and activated alumina have emerged as particularly effective materials due to their availability, high surface area, and strong ion-exchange capacities<sup>3,12</sup>.

Numerous adsorbents have been investigated for water hardness removal through batch adsorption experiments. Gholikandi et al. studied natural zeolite modified with surfactants and demonstrated enhanced removal efficiencies for hardness ions<sup>13</sup>. Yusof et al. examined sodium- and potassium-modified zeolites, observing improved calcium ion adsorption capacities<sup>14</sup>. Noori Sepehr et al. utilized modified pumice stones, achieving removal efficiencies of up to 94% for calcium and 73% for magnesium ions<sup>15</sup>. Abdollahnejad et al. tested Iranian natural zeolite and blast furnace slag as slow sand filters, proving their effectiveness for small-scale community water softening applications<sup>16</sup>. Furthermore, Kumari et al. demonstrated the efficiency of acid-activated alumina for contaminant removal, emphasizing the potential of surface-modified ceramic materials<sup>17</sup>.

In recent years, a few studies have extended this work to continuous-flow and novel adsorption systems. For instance, Salam et al. achieved over 90% removal of Ca<sup>2+</sup> and Mg<sup>2+</sup> using a synthetic muscovite-based sodalite in

<sup>1</sup>Faculty of Petroleum, Gas and Petrochemical Engineering, Department of Chemical Engineering, Persian Gulf University, Bushehr, Iran. <sup>2</sup>Division of Water Environment Technology, Department of Architecture and Civil Engineering, Chalmers University of Technology, Gothenburg, Sweden. <sup>3</sup>Department of Engineering, University of Exeter, Exeter, UK. ✉email: m.abbasi@pgu.ac.ir

a lab-scale fixed-bed column<sup>18</sup>. Kaewmee et al. reported maximum Ca<sup>2+</sup> and Mg<sup>2+</sup> adsorption capacities of 52.0 mg/g and 17.3 mg/g, respectively, using a potassium-activated fly ash geopolymer adsorbent<sup>19</sup>. Ghanbarizadeh et al. observed that natural clinoptilolite zeolite (NaCl-treated) could reduce water hardness by as much as 93% in drinking water treatment<sup>3</sup>. Similarly, Mubarak et al. demonstrated effective simultaneous removal of hardness and heavy metals using a TiO<sub>2</sub>-impregnated zeolite 4 A nanocomposite in both batch and column modes<sup>20</sup>. More advanced treatment systems have also been explored: Ali et al. achieved ~ 80% Ca<sup>2+</sup> removal (alongside near-complete heavy metal and nitrate removal) using a magnetic biochar-based bioceramsite reactor under continuous flow<sup>21</sup>.

Although previous studies have demonstrated the potential of ceramic adsorbents, particularly modified zeolite and alumina, for water hardness removal, these investigations have predominantly been limited to batch adsorption experiments conducted under laboratory conditions. Consequently, there is a critical knowledge gap regarding the performance, operational feasibility, and scalability of these modified adsorbents in continuous fixed-bed column systems. Moreover, the influence of key operational parameters such as adsorbent type, flow rate, and column dimensions on adsorption efficiency has not been sufficiently explored or modeled at pilot scale. Addressing these gaps is essential to translate laboratory findings into practical applications for sustainable water treatment.

To address these research gaps, the current study investigates the removal of water hardness (Ca<sup>2+</sup> and Mg<sup>2+</sup> ions) using a continuous fixed-bed adsorption system with natural zeolite and activated alumina modified by NaNO<sub>3</sub> and H<sub>2</sub>SO<sub>4</sub>, respectively. Unlike previous batch studies, this work represents one of the first attempts to assess modified ceramic adsorbents under continuous, pilot-scale conditions. The main objective is to evaluate how adsorbent type, column diameter, and flow rate influence hardness removal efficiency, as well as to model adsorption behavior using kinetic models including Thomas, Yoon–Nelson, and Adams–Bohart. This approach provides essential insights into the practical applicability and scalability of modified ceramic adsorbents for effective water softening.

## Materials and methods

### Adsorbents and materials

In this study, two types of adsorbents were used to reduce the hardness of drinking water: natural zeolite (clinoptilolite type) and activated alumina. The zeolite was obtained from Afrazand Company (Tehran, Iran), and the activated alumina was sourced from the Iranian Institute of Research & Development in Chemical Industries (Karaj, Iran). Key characteristics of both materials are summarized in Table 1. Before use, the adsorbents were thoroughly washed with distilled water until the total dissolved solids (TDS) in the rinse water reached levels comparable to those of pure distilled water. The materials were then dried in an oven at 55 °C for 24 h.

An ammonia buffer solution was employed in the experiment to determine water hardness through complexometric titration. The buffer solution consisted of 32% ammonia solution, 99.8% pure ammonium chloride, 99.5% pure magnesium sulfate, and 99.8% pure EDTA. For hardness titration, sodium hydroxide (99.5% purity) and Eriochrome Black T reagent (C<sub>20</sub>H<sub>12</sub>N<sub>3</sub>O<sub>7</sub>SNa, 99.8% purity) were used. In addition, reagents Murexide or Ammonium Purate (NH<sub>4</sub>C<sub>8</sub>H<sub>4</sub>N<sub>5</sub>O<sub>6</sub> or C<sub>8</sub>H<sub>5</sub>N<sub>5</sub>O<sub>6</sub>NH<sub>3</sub>, 99.5% purity) were employed for complexometric titration, specifically for calcium ion determination (as a water hardness agent). Ethylenediaminetetraacetic acid (EDTA, 99.8% purity) and 98% concentrated sulfuric acid (H<sub>2</sub>SO<sub>4</sub>) were also used. It is noteworthy that sulfuric acid was supplied by Iran's Pars Chemical Company, while all other chemical materials were obtained from Merck Company, Germany.

### Characterization of adsorbents

The characteristics of the utilized adsorbents were determined through various analytical techniques. X-Ray Diffraction analysis (XRD) was conducted using an X-ray diffractometer (Bruker, D8 Advance, Germany) to identify their crystallographic patterns. Scanning Electron Microscopy (SEM) was employed using a TESCAN instrument (Brno, Czech Republic) to examine the surface morphological characteristics. The specific surface area, crucial for adsorption capacity, was analyzed using the Brunauer–Emmett–Teller (BET) method, and

| Adsorbent         | Composition                    | Content (wt%) |
|-------------------|--------------------------------|---------------|
| Zeolite           | SiO <sub>2</sub>               | 68.5%         |
|                   | Al <sub>2</sub> O <sub>3</sub> | 11%           |
|                   | Na <sub>2</sub> O              | 3.8%          |
|                   | K <sub>2</sub> O               | 4.4%          |
|                   | CaO                            | 0.6%          |
|                   | Fe <sub>2</sub> O <sub>3</sub> | 0.2%          |
|                   | Loss on ignition (L.O.I)       | 11.5%         |
| Activated alumina | Al <sub>2</sub> O <sub>3</sub> | 6%            |
|                   | L.O.I                          | 6%            |
|                   | Na <sub>2</sub> O              | 0.35%         |
|                   | Fe <sub>2</sub> O <sub>3</sub> | 0.02%         |
|                   | SiO <sub>2</sub>               | 0.02%         |

**Table 1.** Characteristics of natural zeolite clinoptilolite and activated alumina.

|                | Parameters     | Unit                      | Values |
|----------------|----------------|---------------------------|--------|
| Drinking water | Total hardness | (mg/L CaCO <sub>3</sub> ) | 520    |
|                | TDS            | (mg/L)                    | 627    |
|                | EC             | (μS/cm)                   | 1248   |
|                | Calcium        | (mg/L)                    | 128.13 |
|                | Magnesium      | (mg/L)                    | 48.6   |
|                | pH             | -                         | 7.72   |

**Table 2.** Drinking water sample analysis.

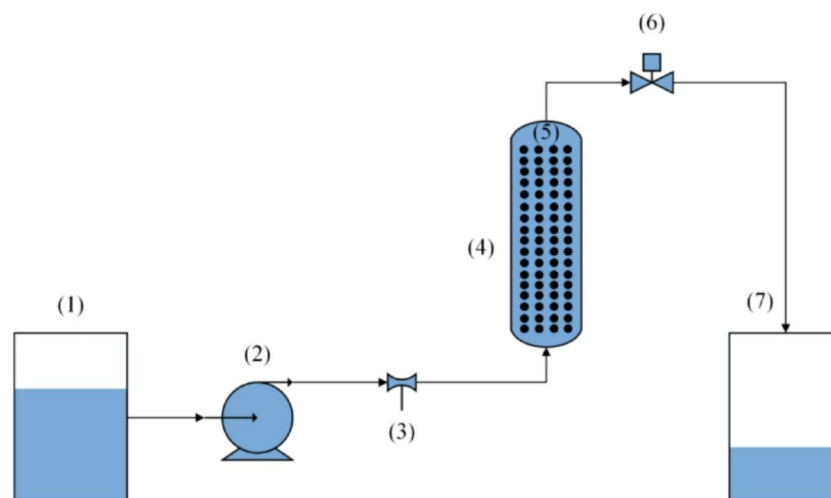


**Fig. 1.** A schematic of the laboratory set-up plant. (1) Input Feed, (2) Pump, (3) Water Flow Meter, (4) Fixed-bed Column, (5) Adsorbent, (6) Sampling Valve, (7) Final Product Tank.

this measurement was performed with a Micromeritics instrument (Micromeritics Corporate Headquarters, Norcross, GA, USA). Fourier Transform Infrared (FTIR) spectroscopy was utilized to determine the functional groups present on the surface of the adsorbents. The FTIR analysis was conducted using a JASCO FTIR 4600 instrument from Japan. Additionally, the surface charge of the adsorbents was evaluated through zeta potential analysis at neutral pH (pH = 7) using a Zeta Compact analyzer (CAD Instrument, France) to provide insight into the electrostatic interactions during adsorption.

### Water samples

In this study, drinking water samples were collected from Bushehr city, Iran. The results of the water analysis are presented in Table 2.

### Adsorption experiments

This study involved the individual evaluation of each adsorbent's performance through a series of controlled experiments. For each adsorbent, total hardness, calcium hardness, and magnesium hardness were determined using the titration method. All adsorption experiments were carried out continuously and divided into two phases.

In the first phase, illustrated in Fig. 1, the laboratory setup was used to assess the ability of the adsorbents to reduce calcium and magnesium concentrations in drinking water. The adsorbents were packed into columns with varying quantities (30 g and 80 g) and column diameters (1 cm and 1.5 cm). The flow rates were set at 10 ml/min and 20 ml/min, and samples were collected at different time intervals. Each collected sample was filtered using Whatman Grade 42 filter paper (Germany) to prepare it for subsequent analysis. The resulting data were then compared against several adsorption column kinetic models to evaluate model fit and predictive accuracy.

In the second phase, modification procedures were applied under the same experimental conditions for both adsorbents. The zeolite adsorbent was modified using a 3 M sodium nitrate (NaNO<sub>3</sub>) solution. It was placed in a beaker containing the solution and stirred for 3 h. Afterward, the sodium nitrate solution was discarded, and the zeolite was rinsed repeatedly with distilled water until a neutral pH was achieved. The adsorbent was then dried in an oven at 55 °C for 24 h.

For activated alumina, modification was performed using 98% sulfuric acid. The adsorbent was mixed with sulfuric acid at a weight-to-volume ratio of 1:3 (activated alumina in grams to H<sub>2</sub>SO<sub>4</sub> in milliliters). The mixture was stirred slowly for 30 min using a mechanical stirrer. Similar to the zeolite procedure, the acid was removed,

and the adsorbent was washed several times with distilled water to reach a neutral pH. Drying was completed in an oven at 105 °C for 4 h.

All prepared adsorbents were collected, properly labeled, and stored in sealed containers to preserve their integrity for further use. Each adsorption experiment was conducted in triplicate to ensure repeatability. The data presented in the manuscript represent the average values from three independent tests. The variation between replicates was 3% across all conditions.

In each experiment, the following equation was utilized to calculate the removal of hardness ions, specifically calcium and magnesium:

$$\text{Removal Efficiency} = \frac{C_i - C_f}{C_i} \times 100 \quad (1)$$

Where  $C_i$  and  $C_f$  (mg/L) indicate the starting and ending concentrations of calcium and magnesium ions in the solution, respectively. The quantity of ions adsorbed by the adsorbent at a given time  $t$  was calculated using Eq. 2.

$$q_t = (C_i - C_t) \times \frac{V}{m} \quad (2)$$

The amount of calcium and magnesium ions adsorbed per unit mass of adsorbent at time  $t$  is denoted as  $q_t$  (mg/g). The concentration of these ions in the solution at time  $t$  is shown as  $C_t$  (mg/L), the solution volume is  $V$  (L), and the mass of the adsorbent is  $m$  (g).

Indeed, the same equation can be utilized to determine the adsorption capacity at equilibrium, which is often denoted as  $q_e$  (mg/g). At equilibrium, the amount of ions (calcium and magnesium) adsorbed per unit mass of adsorbent reaches a steady state, and the adsorption process stabilizes. The Eq. (3) is used for calculating the adsorption capacity at equilibrium.

$$q_e = (C_i - C_e) \times \frac{V}{m} \quad (3)$$

where the concentration of ions (calcium and magnesium) in the solution at the equilibrium time is denoted by  $C_e$  (mg/l).

## Measurement of target parameters

### Measurement of total hardness

The water analysis process began by adding 15 ml of drinking water into a 250 ml Erlenmeyer flask. To maintain a constant pH, 1 cc of ammonium buffer was added to the sample. A few drops of Eriochrome Black T reagent were then introduced. At a pH of approximately 10, Eriochrome Black T forms a red complex with calcium and magnesium cations. EDTA was subsequently added to the solution, breaking the complex and releasing Eriochrome Black T. This reaction causes the solution to change color from red to blue, indicating the endpoint of the titration process. Total hardness was determined in terms of calcium carbonate using Eq. (4)<sup>22</sup>.

$$\text{Total hardness} \left( \frac{\text{mg}}{\text{L}} \right) = \frac{V_c \times f_c \times 10000}{V} \quad (4)$$

In the Eq. (4),  $V_c$  represents the volume of EDTA consumed in the titration process,  $f_c$  denotes the normality of EDTA, and  $V$  (mL) represents the volume of the water sample.

### Measurement of the calcium hardness

To measure calcium hardness, 15 ml of the water sample was carefully transferred into a 250 ml Erlenmeyer flask using a graduated pipette. Subsequently, 1 to 2 drops of 1 N NaOH and an appropriate amount of Murexide reagent were added to the flask, causing the sample to turn pink. The titration process was initiated by using a standard solution of 1 M EDTA until a distinct purple color appeared, indicating the endpoint. The quantity of titrant (EDTA) used during the titration process was recorded. Calcium hardness was then calculated using Eq. (5)<sup>16</sup>. Additionally, Eq. (6) was employed to determine the concentration of calcium ions in the water sample.

$$\text{Calcium hardness} \left( \frac{\text{mg}}{\text{L}} \right) = \frac{V_C \times f_c \times 10000}{V} \quad (5)$$

$$\text{Ca}^{2+} \left( \frac{\text{mg}}{\text{L}} \right) = \text{Calcium hardness as } \frac{\text{mg}}{\text{L}} \text{CaCO}_3 \times 0.4004 \quad (6)$$

### Measurement of magnesium hardness

Magnesium hardness is determined by subtracting the total hardness and calcium hardness values, as specified in Eq. (7)<sup>22</sup>. Additionally, Eq. (8) is employed to calculate the concentration of magnesium ions in the water sample.

$$\text{Magnesium hardness (mg/L)} = \text{Total hardness} - \text{Calcium hardness} \quad (7)$$

$$\text{Mg}^{2+} \left( \frac{\text{mg}}{\text{L}} \right) = (\text{Total hardness} - \text{Calcium hardness}) \times 0.243 \quad (8)$$

## Kinetic models of adsorption columns

Three kinetic models were applied to analyze the fixed-bed adsorption performance: the Thomas, Yoon–Nelson, and Adams–Bohart models. These models help describe the dynamic behavior of ion adsorption in continuous systems and estimate model parameters relevant to column performance.

The Thomas model, developed on the basis of mass transfer theory<sup>23</sup>, is widely applied to evaluate the adsorption capacity of an adsorbent and to determine the Thomas model constant ( $k_{th}$ ) using experimental data from fixed-bed column studies. Both the non-linear and linearized forms of the Thomas model are presented in Eqs. (9) and (10) respectively<sup>24</sup>.

$$\frac{C_t}{C_0} = \frac{1}{1 + e^{K_{th} \left( \frac{Q_{th} m}{Q} - C_0 t \right)}} \quad (9)$$

$$\ln \left( \frac{C_0}{C_t} - 1 \right) = \frac{K_{th} \times Q_{th} \times m}{Q} - K_{th} \times C_0 \times t \quad (10)$$

where  $C_t$  and  $C_0$  are the effluent and influent concentrations (mg/L),  $k_{th}$  is the Thomas model constant (ml min<sup>-1</sup> mg<sup>-1</sup>),  $Q_{th}$  is the adsorption capacity (mg g<sup>-1</sup>),  $m$  is the adsorbent mass (g),  $Q$  is the flow rate (ml min<sup>-1</sup>), and  $t$  is time (min).

The Adams-Bohart model is developed based on the assumption that the adsorption rate is proportional to both the remaining capacity of the adsorbent and the concentration of the adsorbate<sup>25</sup>. This model is particularly suitable for describing the initial part ( $C/C_0 < 0.15$ ) of the breakthrough curve<sup>25</sup>. It has found wide applications in various systems. Both the non-linear and linearized forms of the Adams-Bohart model are presented in Eqs. (11) and (12) respectively<sup>24</sup>.

$$\frac{C_t}{C_0} = \exp(K_{AB} C_0 t - K_{AB} N_0 \frac{Z}{U_0}) \quad (11)$$

$$\ln \left( \frac{C_t}{C_0} \right) = K_{AB} C_0 t - K_{AB} N_0 \frac{Z}{U_0} \quad (12)$$

where  $K_{AB}$  (L mg<sup>-1</sup> min<sup>-1</sup>) is the kinetic constant,  $N_0$  (mg L<sup>-1</sup>) is the concentration of saturation,  $Z$  (cm) is the bed height and  $U_0$  (cm min<sup>-1</sup>) is the linear rate.

The Yoon-Nelson model is widely used in single adsorbent systems due to its simplicity, as it does not require detailed information about the adsorbent and column properties<sup>18</sup>. Both the non-linear and linearized forms of the Yoon-Nelson model are presented in Eqs. (13) and (14) respectively<sup>24</sup>.

$$\frac{C_t}{C_0} = \frac{1}{1 + e^{K_{YN}(\tau - t)}} \quad (13)$$

$$\ln \left( \frac{C_t}{C_0 - C_t} \right) = K_{YN} t - \tau K_{YN} \quad (14)$$

where  $\tau$  (min) is the time of 50% saturation and  $K_{YN}$  (min<sup>-1</sup>) is the rate constant.

## Results and discussion

### Characterization of Zeolite, and activated alumina

#### Scanning electron microscopy (SEM)

SEM images (Figs. 2, 3, 4 and 5) provide visual evidence of surface morphology before and after ion adsorption for natural zeolite, modified zeolite, activated alumina, and modified activated alumina. All samples were imaged at 10,000× magnification.

In natural zeolite (Fig. 2a), the unmodified surface exhibits a rough, layered texture with visible micropores. After adsorption (Fig. 2b), the surface appears smoother, suggesting pore blockage due to ion uptake. The modified zeolite (Fig. 3a) shows greater porosity and surface fragmentation compared to the natural form, which enhances active site accessibility. After ion exchange (Fig. 3b), the surface becomes denser and less porous, indicating successful Ca<sup>2+</sup> and Mg<sup>2+</sup> adsorption.

For activated alumina, the surface prior to adsorption (Fig. 4a) is relatively smooth and granular. Post-adsorption (Fig. 4b), the surface displays coverage of pores and edge softening. In the modified alumina (Fig. 5a), sulfuric acid treatment results in increased roughness and porosity. After adsorption (Fig. 5b), the surface appears coated and compacted, confirming ion capture and partial pore saturation.

These morphological transitions validate the effectiveness of the surface modification treatments in enhancing adsorption efficiency.

#### Brunauer–Emmett–Teller (BET)

BET analysis is utilized to measure the specific surface area of materials by determining the volume of nitrogen gas adsorbed and desorbed at a constant temperature of liquid nitrogen (77°K). In this study, BET analysis was performed to measure the specific surface area of natural zeolite and activated alumina adsorbents, and the results are presented in Figs. 6 and 7. BET surface area, Langmuir surface area, pore volume, and mean pore size of Natural Zeolite before and after adsorption (NZ-BA, NZ-AA) and Activated Alumina before and after adsorption (AA-BA, AA-AA) are reported in Table 3.

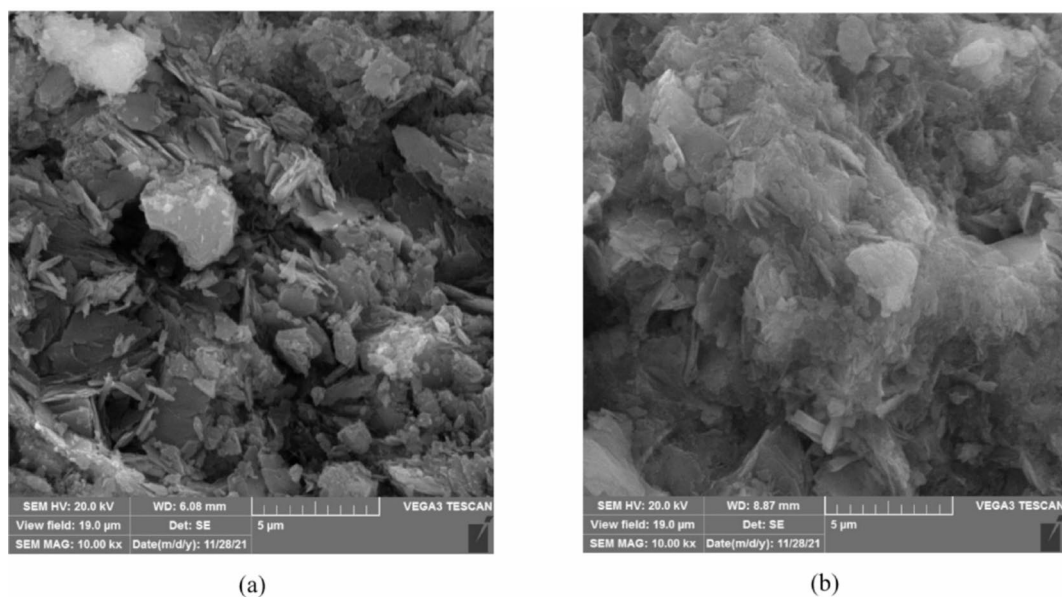


**Fig. 2.** SEM for natural zeolite adsorbent surface at a magnification equal to (10000x) (a) natural zeolite before and (b) after  $\text{Ca}^{2+}$  and  $\text{Mg}^{2+}$  ions adsorption.

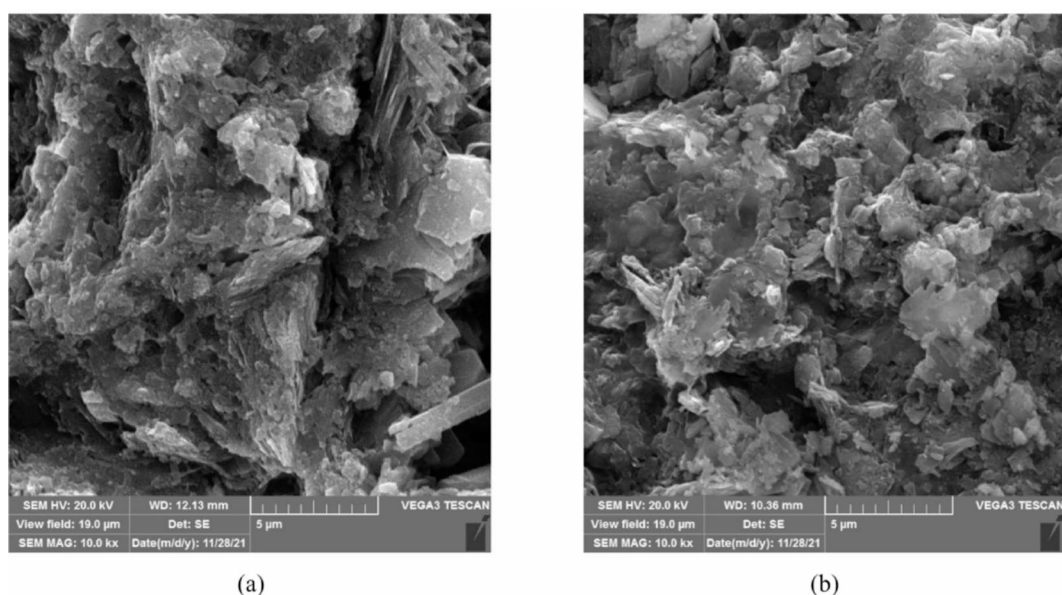


**Fig. 3.** SEM images of modified zeolite adsorbent surface at a magnification equal to (10000x) (a) modified zeolite before and (b) after adsorption of  $\text{Ca}^{2+}$  and  $\text{Mg}^{2+}$  ions.

The BET surface area analysis revealed a significantly higher specific surface area for Activated Alumina (AA) at  $298.24 \text{ m}^2/\text{g}$  compared to Natural Zeolite (NZ) at  $25.26 \text{ m}^2/\text{g}$ . This enhancement is attributed to the activation process, which introduces numerous pores and increases the overall surface area. While NZ may possess a favorable porous structure, its natural state appears to limit the development of a comparable surface area<sup>26,27</sup>.

Nitrogen adsorption-desorption isotherms (Figs. 6a and 7a) demonstrate a progressive increase in nitrogen adsorption with rising relative pressure for both AA and NZ. The isotherms exhibit distinct hysteresis loops, indicative of specific pore size distributions within the respective materials. Pore size analysis (Figs. 6b and 7b) confirms that both AA and NZ exhibit mesoporous characteristics below a pore width of 50 nm. However, AA displays a smaller average pore width of  $51.77 \text{ \AA}$  compared to NZ at  $107.78 \text{ \AA}$ <sup>17</sup>.

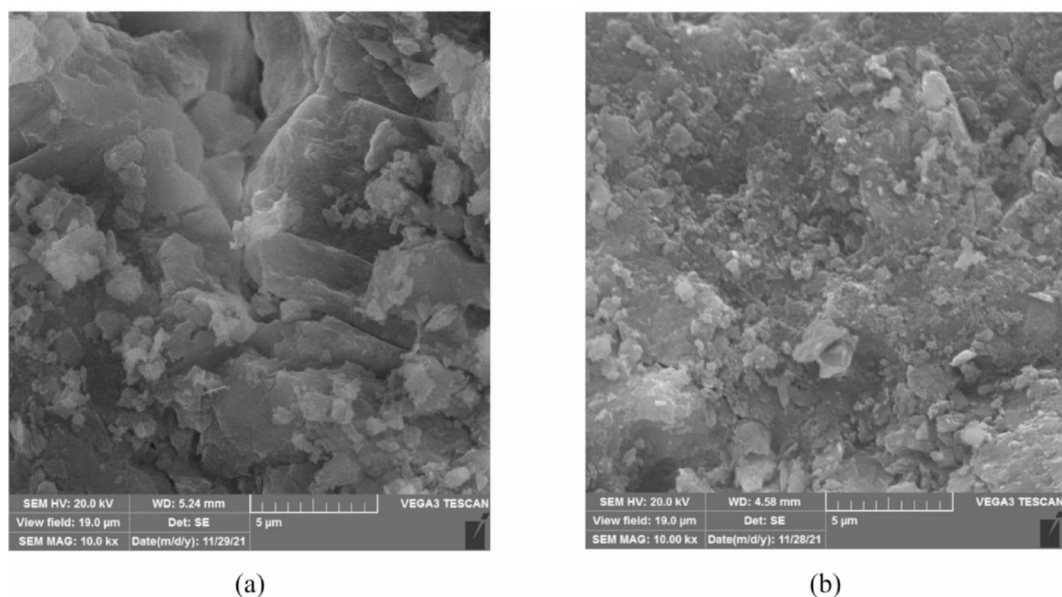


**Fig. 4.** SEM images of the activated alumina adsorbent surface at a magnification equal to (10000x) (a) activated alumina before and (b) after the adsorption of  $\text{Ca}^{2+}$  and  $\text{Mg}^{2+}$  ions.

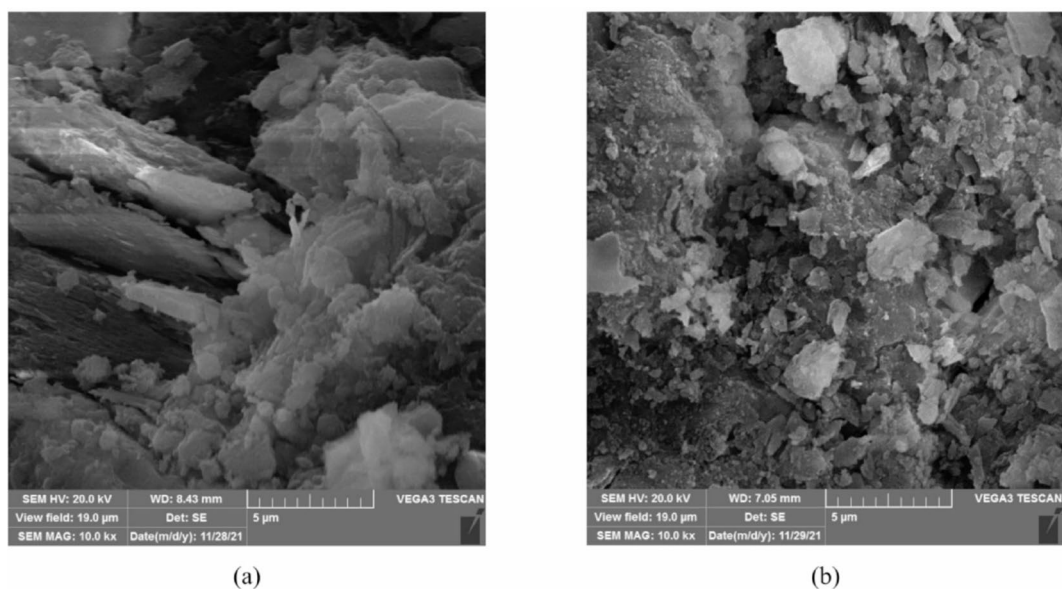


**Fig. 5.** SEM images of modified active alumina adsorbent surface at a magnification equal to (10000x) (a) modified active alumina before and (b) after adsorption of  $\text{Ca}^{2+}$  and  $\text{Mg}^{2+}$  ions.

#### Fourier transform infrared (FTIR)

FTIR spectroscopy was used to identify molecular structures, functional groups, and bonding characteristics in the adsorbents (Figs. 8 and 9). Spectra were recorded in the wavenumber range  $399\text{--}4000\text{ cm}^{-1}$  for natural and modified zeolite, and for activated and modified alumina.

For natural zeolite (Fig. 8), the dominant band at  $1030\text{ cm}^{-1}$  corresponds to Si-O-Si asymmetric stretching, while bands at  $750\text{--}800\text{ cm}^{-1}$  and  $450\text{--}475\text{ cm}^{-1}$  are assigned to Al-O-Al stretching and O-Si-O bending vibrations, respectively. After modification with  $\text{NaNO}_3$ , peak positions remained largely unchanged, but intensities varied, indicating physical adsorption. A new band at  $1384\text{ cm}^{-1}$  appeared, attributed to nitrate incorporation<sup>26</sup>.

For activated alumina (Fig. 9), the broad band at  $3460\text{ cm}^{-1}$  and peaks at  $1634$ ,  $1403$ , and  $1119\text{ cm}^{-1}$  correspond to O-H stretching and bending vibrations. Modification with  $\text{H}_2\text{SO}_4$  increased peak intensities and introduced new bands at  $534$  and  $613\text{ cm}^{-1}$ , characteristic of sulfate adsorption<sup>17</sup>.

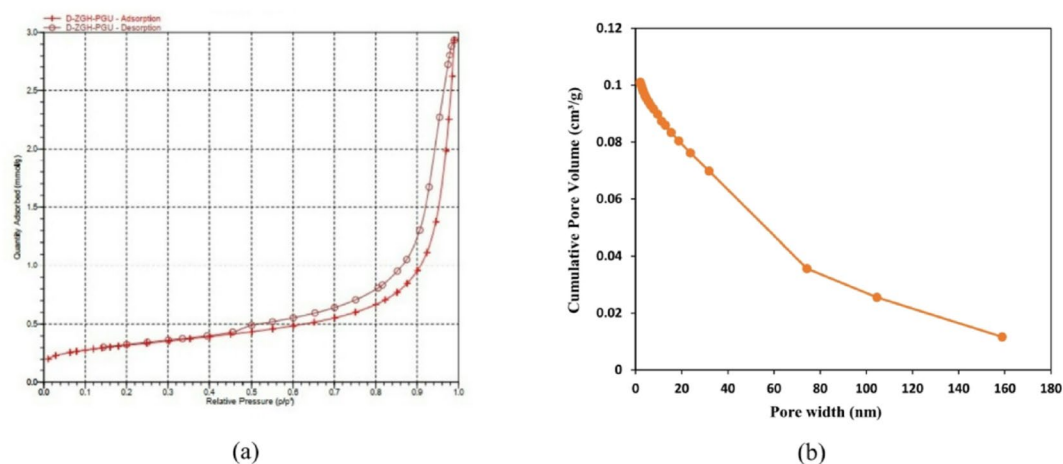


**Fig. 6.** BET analysis of natural zeolite adsorbent surface (a) N<sub>2</sub> adsorption - desorption isotherms of samples, and (b) cumulative pore volume versus pore width distribution.

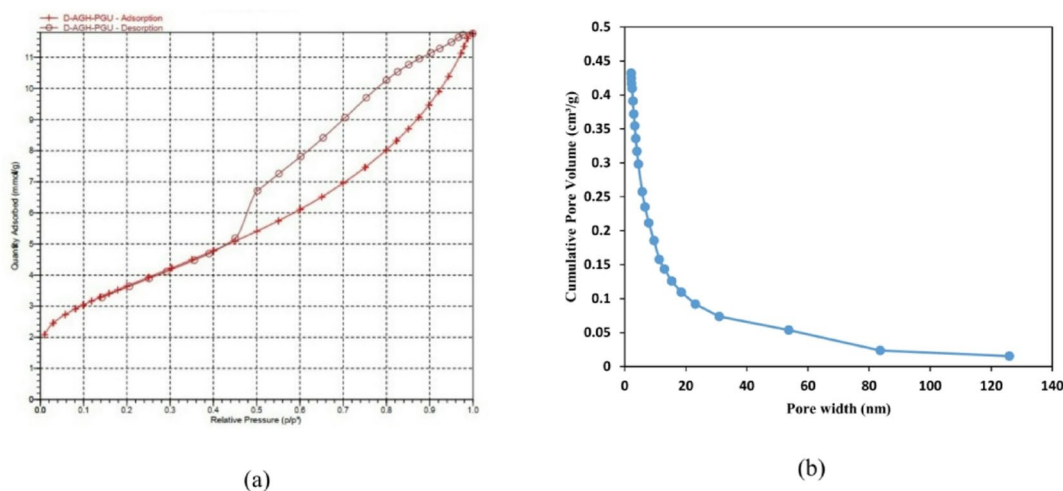


**Fig. 7.** BET analysis of activated alumina adsorbent surface (a) N<sub>2</sub> adsorption - desorption isotherms of samples, and (b) cumulative pore volume versus pore width distribution.

| Parameter                                 | NZ-BA  | NZ-AA  | AA-BA  | AA-AA  |
|---|--------|--------|--------|--------|
| BET surface area (m <sup>2</sup> /g)      | 25.56  | 24.86  | 298.24 | 275.77 |
| Langmuir surface area (m <sup>2</sup> /g) | 35.07  | 33.94  | 413.68 | 382.6  |
| Total pore volume (cm <sup>3</sup> /g)    | 0.069  | 0.075  | 0.386  | 0.38   |
| Average pore width (Å)                    | 107.78 | 121.21 | 51.77  | 54.7   |

**Table 3.** Summary of BET analysis of adsorbent before adsorption.

#### X-Ray diffraction analysis

XRD analysis was conducted to verify the purity of natural zeolite and determine the structural characteristics of activated alumina, as shown in Figs. 10 and 11.

The XRD pattern of natural zeolite shows a sharp peak at  $2\theta \approx 27.1^\circ$ , indicating high crystallinity, along with several smaller peaks between  $2\theta \approx 10^\circ$  and  $35^\circ$ , confirming its polycrystalline nature. These features are consistent with the clinoptilolite phase, which typically exhibits reflections at  $\sim 10^\circ$ ,  $\sim 22.4^\circ$ , and  $\sim 27\text{--}30^\circ$ <sup>28</sup>. The sharp peaks and low background noise indicate good structural integrity and minimal amorphous content, making it suitable for ion-exchange applications.

The XRD pattern of activated alumina reveals broad peaks around  $2\theta \approx 13^\circ$ ,  $28^\circ$ ,  $38^\circ$ ,  $48^\circ$ ,  $66^\circ$ , and  $68^\circ$ , characteristic of  $\gamma\text{-Al}_2\text{O}_3$  (gamma-phase alumina). The absence of sharp peaks suggests a partially crystalline,

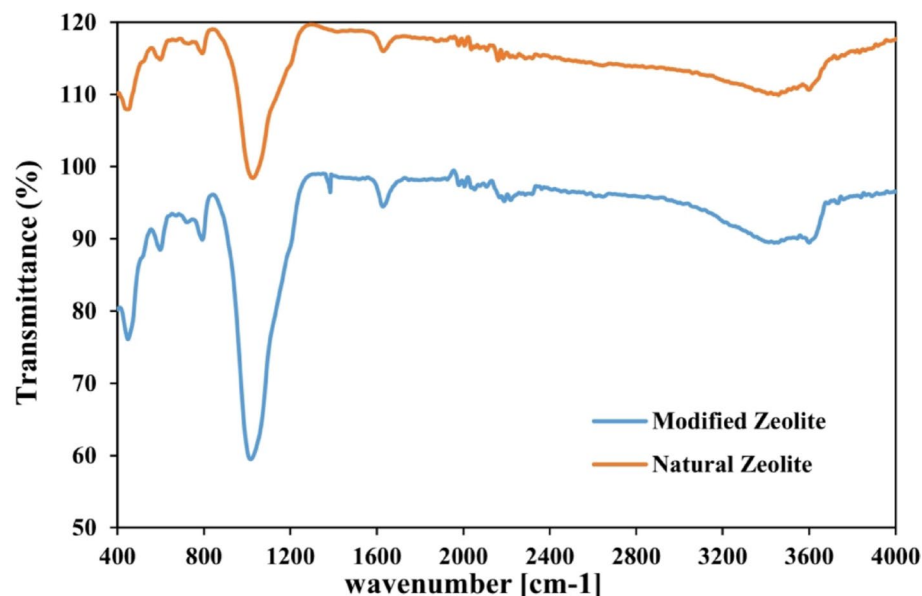


Fig. 8. FTIR analysis of natural and modified zeolite adsorbent.

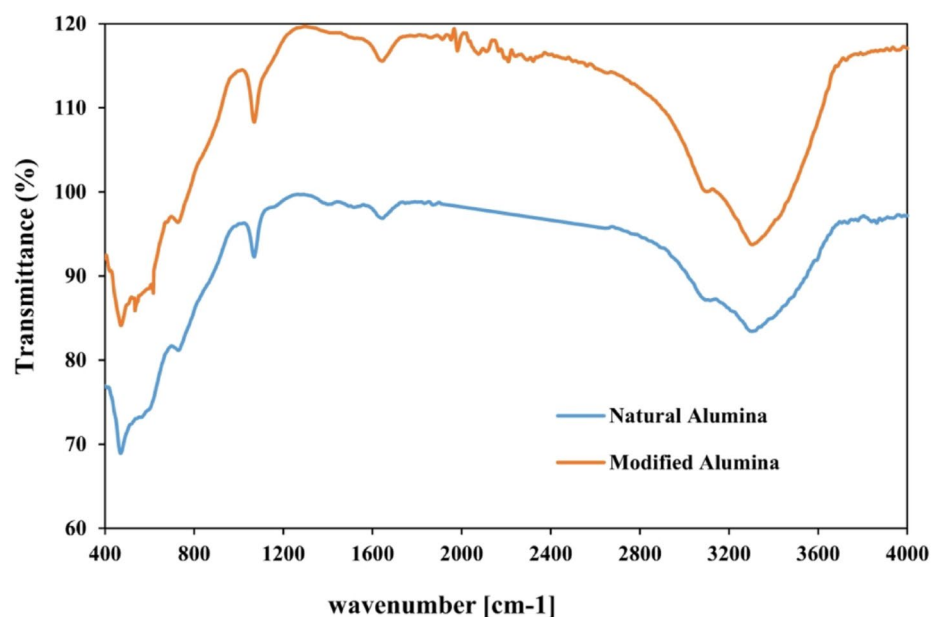


Fig. 9. FTIR analysis of active alumina adsorbent and modified active alumina.

partially amorphous structure with nanocrystalline domains. These results align with literature identifying gamma alumina through broad diffraction features, particularly near  $38^\circ$  and  $46^\circ$ <sup>17</sup>.

#### Zeta potential analysis

Zeta potential measurements were performed to assess the surface charge of the adsorbents at the neutral pH condition (pH 7) used throughout the experiments. The analysis was conducted using a Zeta Compact analyzer (CAD Instrument, France). Results showed that natural zeolite had a zeta potential of  $-24$  mV, indicating a strongly negative surface charge, while activated alumina exhibited a weaker negative charge of  $-4$  mV. These values suggest that zeolite has a greater tendency to attract and exchange divalent cations such as  $\text{Ca}^{2+}$  and  $\text{Mg}^{2+}$  via electrostatic interaction and ion exchange mechanisms.

#### Reducing water hardness with adsorbents and their modified forms

To reduce the hardness of drinking water, natural zeolite of the clinoptilolite type and activated alumina were used as adsorbents. Both materials were subsequently modified to enhance their adsorption performance,

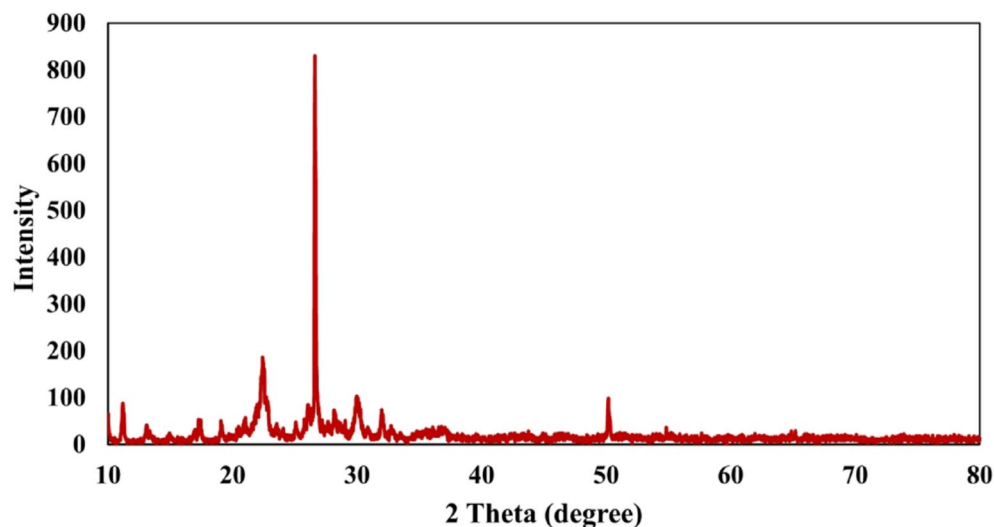


Fig. 10. XRD analysis of natural zeolite.

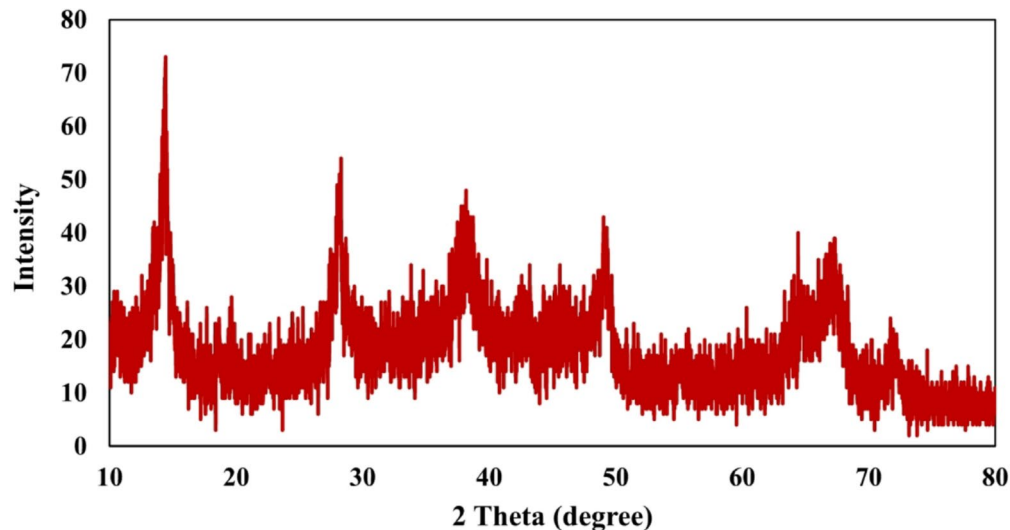


Fig. 11. XRD analysis of activated alumina.

natural zeolite with 3 M sodium nitrate and activated alumina with 98% sulfuric acid. These modifications were intended to improve the efficiency of the adsorbents in removing calcium and magnesium ions from the water. Figure 12 illustrates the proposed adsorption mechanisms responsible for the removal of  $\text{Ca}^{2+}$  and  $\text{Mg}^{2+}$  ions by natural zeolite and activated alumina.

#### *Natural zeolite clinoptilolite type*

Figures 13, 14, 15 and 16 present the removal efficiencies for total hardness, calcium, and magnesium ions at various contact times. The experiments were conducted using two fixed-bed column configurations: one containing 30 g of adsorbent with a 1 cm diameter, and the other containing 80 g of adsorbent with a 1.5 cm diameter. Both systems were operated at ambient temperature, with flow rates of 10 ml/min and 20 ml/min, for a duration of 600 min. The concentrations of total hardness, calcium, and magnesium ions were determined using the complexometric titration method with EDTA.

The results show that both natural and modified zeolite effectively reduced total water hardness, with the modified form demonstrating superior performance. Under optimal conditions, natural zeolite achieved a 96% reduction in total hardness, while modified zeolite reached 99.23%. In terms of calcium removal, both natural zeolite and activated alumina displayed effective adsorption capabilities, and their modified versions exhibited further improvement. Similarly, both adsorbents effectively removed magnesium ions, with the modification process enhancing removal efficiency.

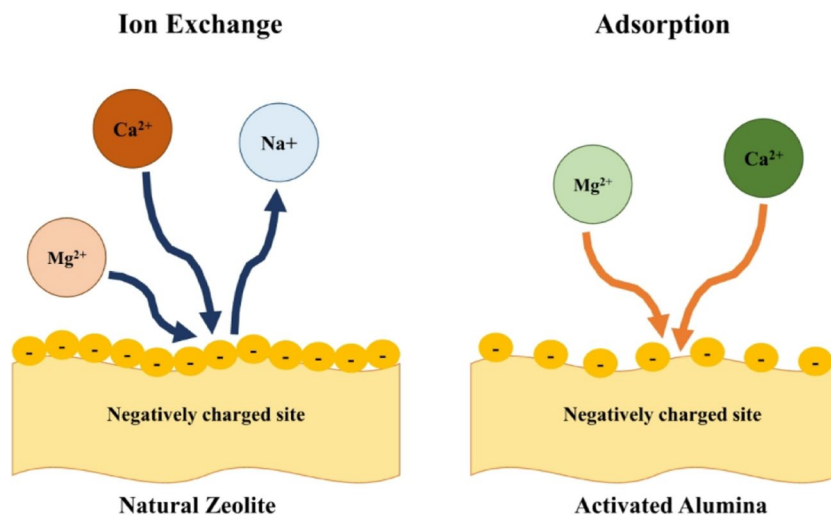


**Fig. 12.** Schematic of adsorption mechanisms for the removal of  $\text{Ca}^{2+}$  and  $\text{Mg}^{2+}$  ions by natural zeolite and activated alumina.

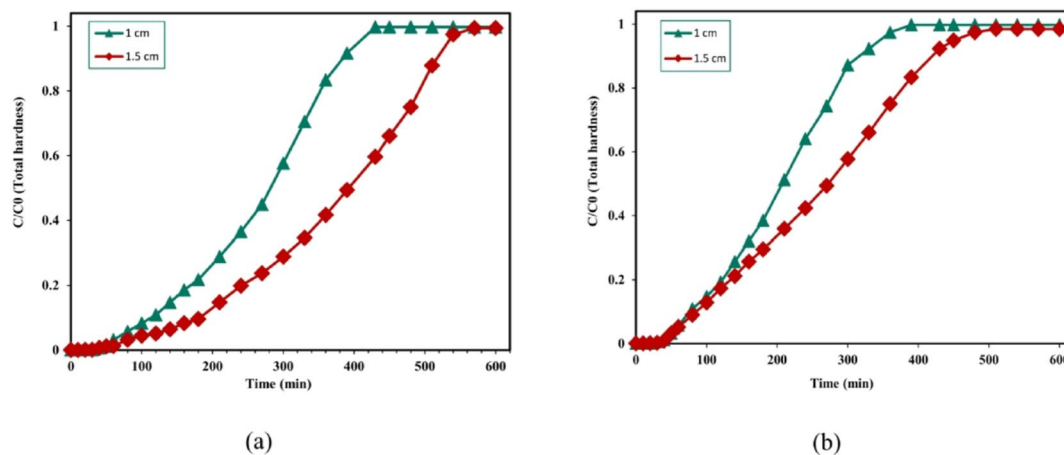


**Fig. 13.** The effect of column diameter and water flow in reducing the total hardness of drinking water by natural zeolite ( $T = 25^\circ\text{C}$ ,  $\text{pH} = 7$ ), (a)  $Q = 10$  ml/min, (b)  $Q = 20$  ml/min.

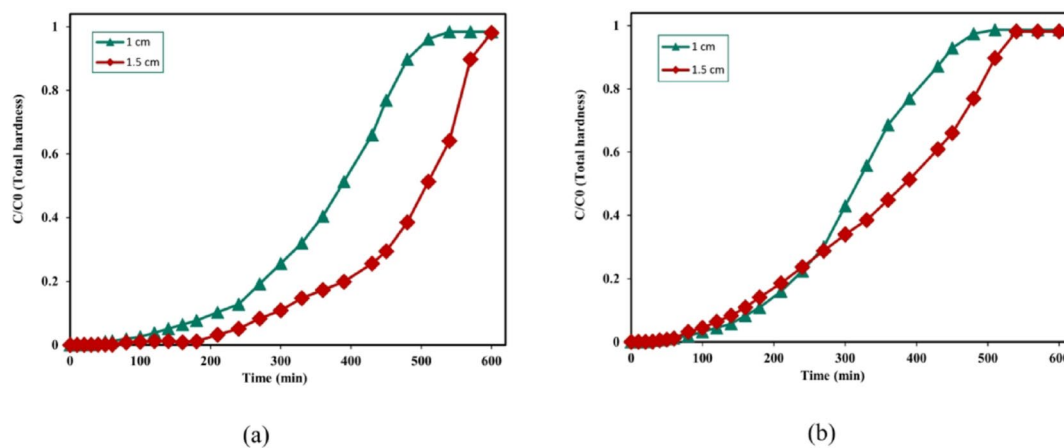


**Fig. 14.** The effect of column diameter and water flow on reducing the total hardness of drinking water by modified zeolite ( $T = 25^\circ\text{C}$ ,  $\text{pH} = 7$ ), (a)  $Q = 10$  ml/min, (b)  $Q = 20$  ml/min.

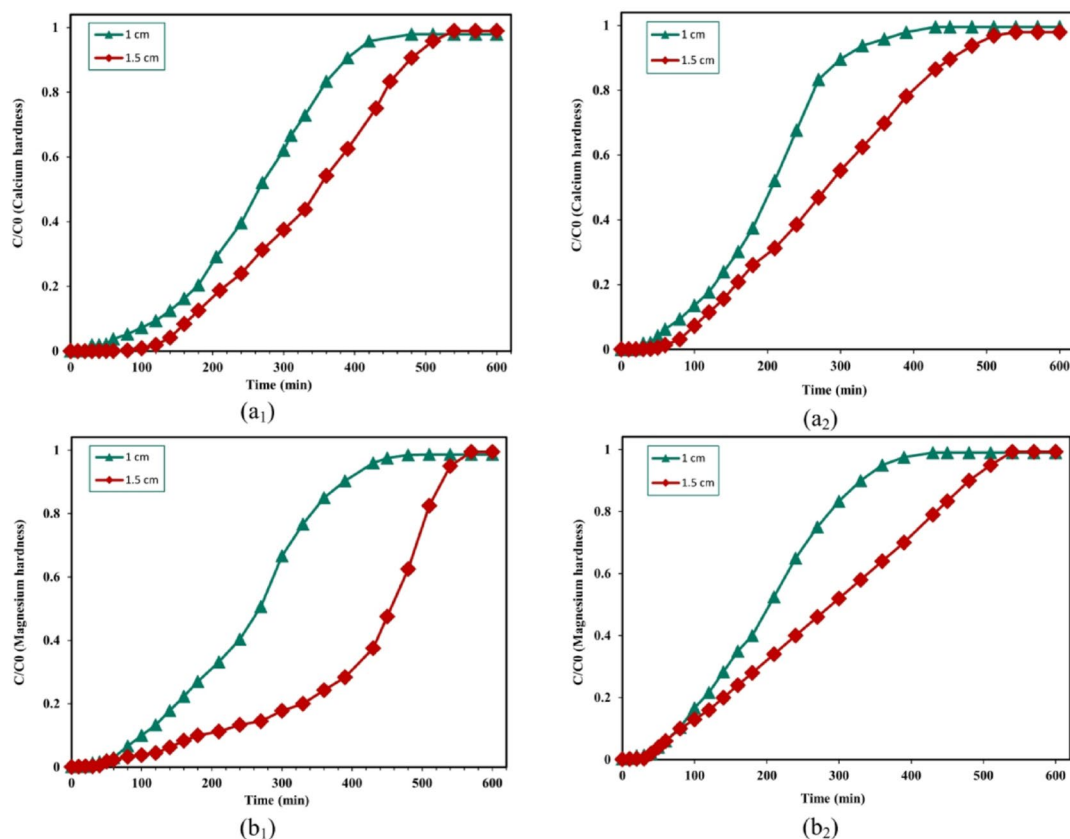


**Fig. 15.** The effect of column diameter and water flow on reducing (a) calcium hardness, and (b) magnesium hardness of drinking water by natural zeolite ( $T = 25^{\circ}\text{C}$ ,  $\text{pH} = 7$ ), ( $a_1, b_1$ )  $Q = 10$  ml/min, ( $a_2, b_2$ )  $Q = 20$  ml/min.

**Investigating the effect of zeolite ion exchange in reducing total hardness** Figure 13 shows the effect of column diameter and flow rate on the performance of fixed-bed columns using natural zeolite to remove total hardness, calcium, and magnesium ions from drinking water. Experiments were conducted at  $\text{pH} 7$  and  $25^{\circ}\text{C}$ , with initial concentrations of total hardness, calcium, and magnesium at  $520$  mg/L,  $320$  mg/L, and  $200$  mg/L, respectively, over  $600$  min.

Increasing the column diameter significantly improved both bed lifetime and overall removal efficiency. At a flow rate of  $10$  ml/min, breakthrough times were  $80$  min for the  $1$  cm column and  $120$  min for the  $1.5$  cm column. At  $20$  ml/min, breakthrough occurred earlier— $50$  min for the  $1$  cm column and  $80$  min for the  $1.5$  cm column. Larger column diameters also resulted in longer saturation intervals.

Bed saturation times were  $430$  min ( $1$  cm) and  $570$  min ( $1.5$  cm) at  $10$  ml/min, and  $390$  min ( $1$  cm) and  $510$  min ( $1.5$  cm) at  $20$  ml/min. The longer saturation times with larger diameters are due to the greater volume of adsorbent, which delays breakthrough and extends treatment time. In contrast, higher flow rates shorten the contact time between water and adsorbent, accelerating saturation and reducing operational duration.

Overall, the optimal conditions for total hardness removal were achieved with a  $1.5$  cm column diameter and a  $10$  ml/min flow rate over a  $600$ -minute period.

**Investigating the effect of ion exchange of modified zeolite in reducing total hardness** To increase adsorption capacity and extend the bed saturation time, the natural zeolite adsorbent was modified using  $3$  M sodium nitrate. The test conditions were identical to those used in the unmodified zeolite experiments, and the results are presented in Fig. 14.

The modified zeolite showed a clear improvement in adsorption performance. At a flow rate of  $10$  ml/min, breakthrough times increased to  $180$  min for the  $1$  cm column and  $240$  min for the  $1.5$  cm column. At  $20$  ml/min, breakthrough occurred at  $120$  min and  $140$  min, respectively.

Saturation times also increased compared to the unmodified zeolite. At  $10$  ml/min, bed saturation occurred at  $540$  min ( $1$  cm) and  $600$  min ( $1.5$  cm). At  $20$  ml/min, saturation was reached at  $510$  min and  $540$  min, respectively. These results confirm that the combination of a larger column diameter and zeolite modification substantially extends the effective adsorption period.

This improvement can be explained by the cation exchange process, in which sodium ions from  $\text{NaNO}_3$  replace exchangeable ions in the zeolite. As a result, the adsorption sites become uniformly occupied by sodium ions, enhancing the material's capacity to remove calcium and magnesium from drinking water.

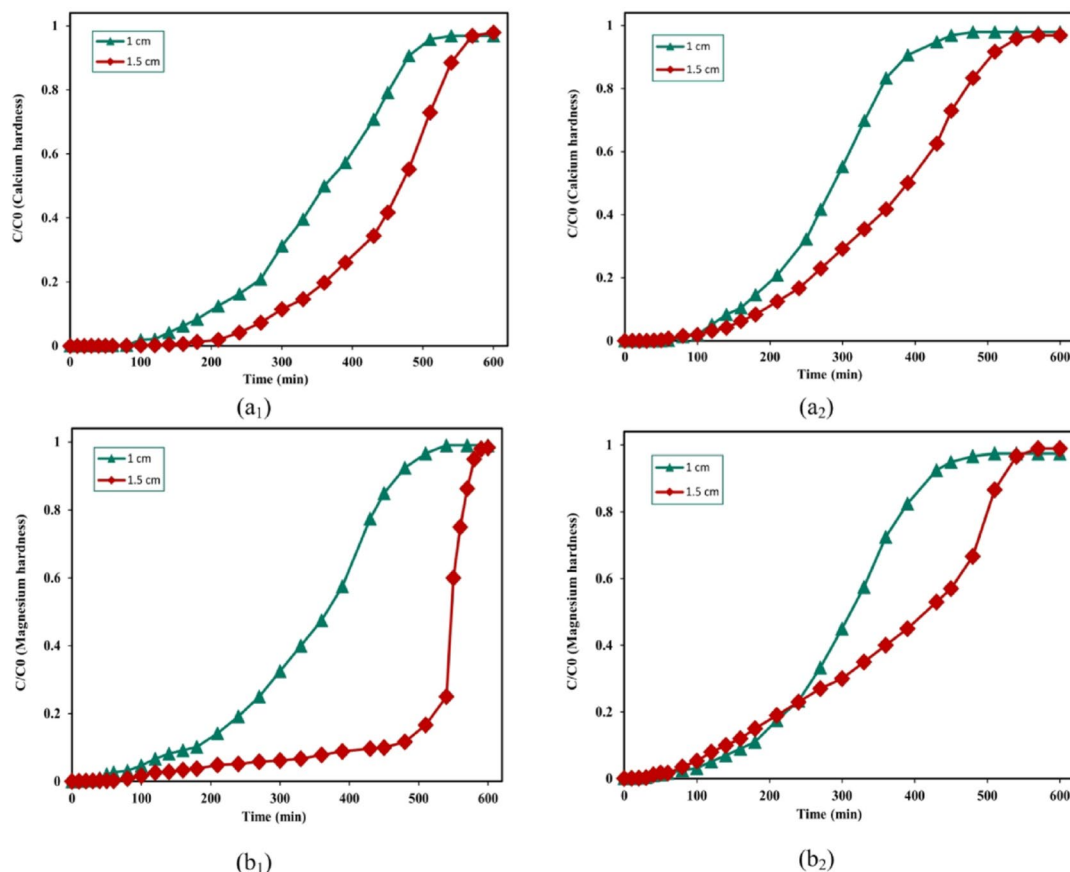


**Fig. 16.** The effect of column diameter and water flow on reducing (a) calcium hardness, and (b) magnesium hardness of drinking water by modified zeolite ( $T = 25^{\circ}\text{C}$ ,  $\text{pH} = 7$ ), ( $a_1, b_1$ )  $Q = 10$  ml/min, ( $a_2, b_2$ )  $Q = 20$  ml/min.

**Investigating the effect of natural zeolite ions exchange in reducing calcium and magnesium ions** Figure 15 illustrates the effect of column diameter and flow rate on calcium and magnesium hardness removal using natural zeolite.

For calcium hardness, the breakthrough times were 60 min (1 cm) and 120 min (1.5 cm) at a flow rate of 10 ml/min, and 40 min and 60 min, respectively, at 20 ml/min. The saturation times were 480 min (1 cm) and 540 min (1.5 cm) at 10 ml/min, and 430 min and 520 min at 20 ml/min. Larger column diameters extended the saturation period, while higher flow rates reduced it.

For magnesium hardness, breakthrough occurred at 60 min (1 cm) and 110 min (1.5 cm) at 10 ml/min, and at 20 min and 40 min, respectively, at 20 ml/min. The corresponding saturation times were 480 min and 540 min at 10 ml/min, and 430 min and 520 min at 20 ml/min. As with calcium, larger diameters increased adsorption duration, whereas higher flow rates accelerated saturation.

These results can be explained by the ion exchange mechanism: as water passes through the NaX form of the zeolite, calcium and magnesium cations are exchanged for sodium ions. Once all sodium ions are replaced by calcium and magnesium, the bed reaches saturation.

**Investigating the effect of modified zeolite ions exchange in reducing calcium and magnesium ions** Figure 16 shows the performance of modified zeolite in removing calcium and magnesium hardness from drinking water. The results indicate a substantial improvement in adsorption capacity compared to the unmodified material.

For calcium hardness, breakthrough times were 100 min (1 cm) and 180 min (1.5 cm) at a flow rate of 10 ml/min, and 80 min for both diameters at 20 ml/min. Bed saturation occurred at 540 min (1 cm) and 600 min (1.5 cm) at 10 ml/min, and 480 min for both columns at 20 ml/min.

For magnesium hardness, breakthrough occurred at 180 min (1 cm) and 450 min (1.5 cm) at 10 ml/min, and 80 min for both diameters at 20 ml/min. Saturation times were 540 min (1 cm) and 600 min (1.5 cm) at 10 ml/min, and 510 min for both diameters at 20 ml/min.

The increased adsorption capacity is attributed to a higher number of active sites, particularly sodium ions introduced through modification, which promote faster ion exchange and extend saturation time. Overall, the modified zeolite improved calcium and magnesium removal efficiency from 95% to 99.17%, making it a more effective adsorbent for hardness reduction in drinking water.

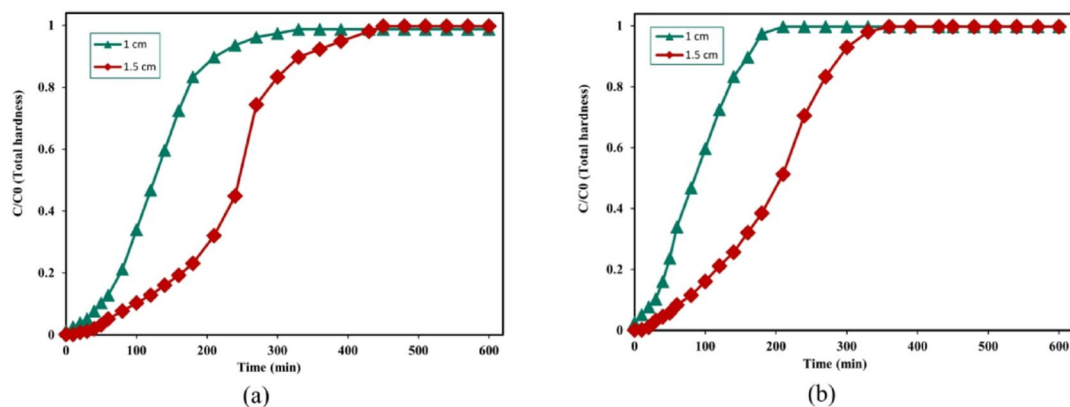


**Fig. 17.** The effect of column diameter and water flow on reducing the total hardness of drinking water by activated alumina ( $T = 25^{\circ}\text{C}$ ,  $\text{pH} = 7$ ), (a)  $Q = 10$  ml/min, (b)  $Q = 20$  ml/min.

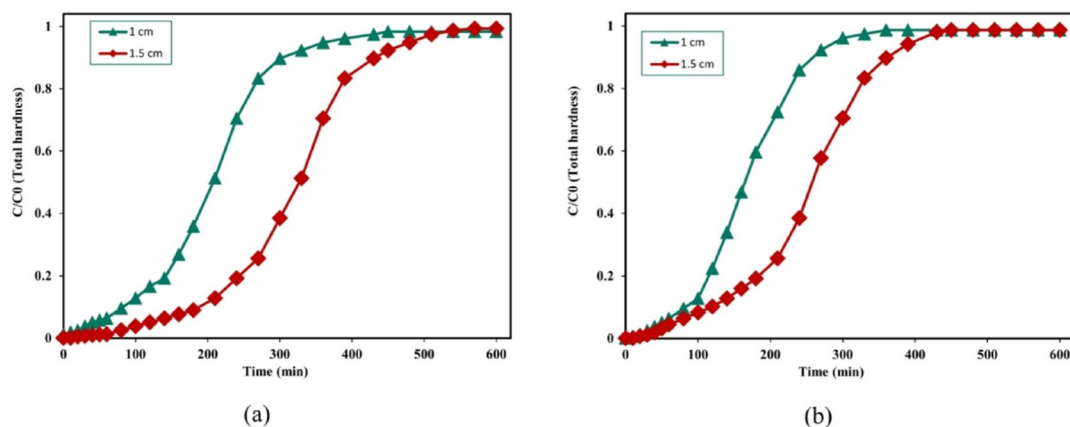


**Fig. 18.** The effect of column diameter and water flow rate on reducing the total hardness of drinking water by modified activated alumina ( $T = 25^{\circ}\text{C}$ ,  $\text{pH} = 7$ ), (a)  $Q = 10$  ml/min, (b)  $Q = 20$  ml/min.

#### Activated alumina

In this stage of the study, activated alumina and its modified form were evaluated as adsorbents for reducing the hardness of drinking water by removing calcium and magnesium ions. The experimental conditions were kept identical to those used for the zeolite tests.

Columns with diameters of 1 cm and 1.5 cm were operated at flow rates of 10 ml/min and 20 ml/min. All experiments were conducted at pH 7 and  $25^{\circ}\text{C}$ , with initial concentrations of total hardness, calcium, and magnesium at 520 mg/L, 320 mg/L, and 200 mg/L, respectively. The contact time for each experiment was 600 min.

**Investigating the effect of activated alumina in reducing total hardness** Figure 17 illustrates the effect of column diameter and flow rate on the performance of activated alumina in reducing total hardness. Increasing the column diameter extended bed lifetime and improved removal efficiency, whereas increasing the flow rate had the opposite effect.

At a flow rate of 10 ml/min, breakthrough occurred at 20 min (1 cm) and 50 min (1.5 cm). At 20 ml/min, breakthrough times were reduced to 10 min and 30 min, respectively. Bed saturation times were 330 min (1 cm) and 450 min (1.5 cm) at 10 ml/min, and 210 min (1 cm) and 360 min (1.5 cm) at 20 ml/min.

This behavior is explained by contact time differences: higher flow rates reduce the interaction between water and the adsorbent bed, leading to earlier saturation, whereas lower flow rates allow for more effective adsorption and a longer bed lifetime.

Overall, the best performance for total hardness reduction was achieved with a 1.5 cm column diameter and a 10 ml/min flow rate over a 600-minute period, providing an optimal balance between contact time and operational duration.

**Investigating the effect of modified activated alumina in reducing total hardness** Figure 18 shows the effect of modifying activated alumina with sulfuric acid on its performance in reducing total hardness. The modification produced only a modest improvement, increasing total hardness removal from 95% to 98.71%. One possible

reason for this limited effect is partial dissolution of activated alumina in sulfuric acid. This was evident as the water samples turned white after each test with the modified adsorbent, requiring filtration through paper to remove turbidity before titration.

At a flow rate of 10 ml/min, breakthrough occurred at 50 min (1 cm) and 180 min (1.5 cm). At 20 ml/min, breakthrough times were 40 min and 140 min, respectively. Bed saturation times were 450 min (1 cm) and 570 min (1.5 cm) at 10 ml/min, and 360 min (1 cm) and 450 min (1.5 cm) at 20 ml/min.

These results suggest that sulfuric acid modification does not significantly enhance the adsorption capacity of activated alumina for total hardness removal. Alternative chemical modifiers may be required to achieve more substantial performance improvements. Further investigation with different modification agents could potentially lead to higher adsorption efficiency.

**Investigating the effect of activated alumina in reducing calcium and magnesium ions** Figure 19 presents the performance of activated alumina in removing calcium and magnesium hardness from drinking water. The results show that adsorption capacity increased with column diameter but decreased with flow rate. Larger columns provided greater surface area for adsorption, enhancing removal efficiency, while higher flow rates reduced contact time between water and the adsorbent, lowering capacity.

Calcium removal was consistently higher than magnesium removal, which can be explained by differences in ion hydration energy. Magnesium ions have a higher charge density than calcium ions, resulting in stronger hydration. During ion exchange, hydrated ions must shed water molecules; because magnesium retains its hydration shell more strongly, it is less likely to be exchanged, leading to lower adsorption.

For calcium hardness, breakthrough occurred at 60 min (1 cm) and 100 min (1.5 cm) at 10 ml/min, and 10 min and 60 min, respectively, at 20 ml/min. Bed saturation times were 360 min (1 cm) and 510 min (1.5 cm) at 10 ml/min, and 430 min and 540 min at 20 ml/min.

For magnesium hardness, breakthrough occurred at 60 min (1 cm) and 180 min (1.5 cm) at 10 ml/min, and 20 min and 40 min, respectively, at 20 ml/min. Bed saturation times were 510 min (1 cm) and 570 min (1.5 cm) at 10 ml/min, and 430 min and 540 min at 20 ml/min.

These findings demonstrate the effectiveness of activated alumina for removing both calcium and magnesium hardness, and emphasize the influence of column diameter and flow rate on adsorption performance.

**Investigating the effect of modified activated alumina in reducing calcium and magnesium ions** Figure 20 illustrates the performance of modified activated alumina in removing calcium and magnesium hardness from

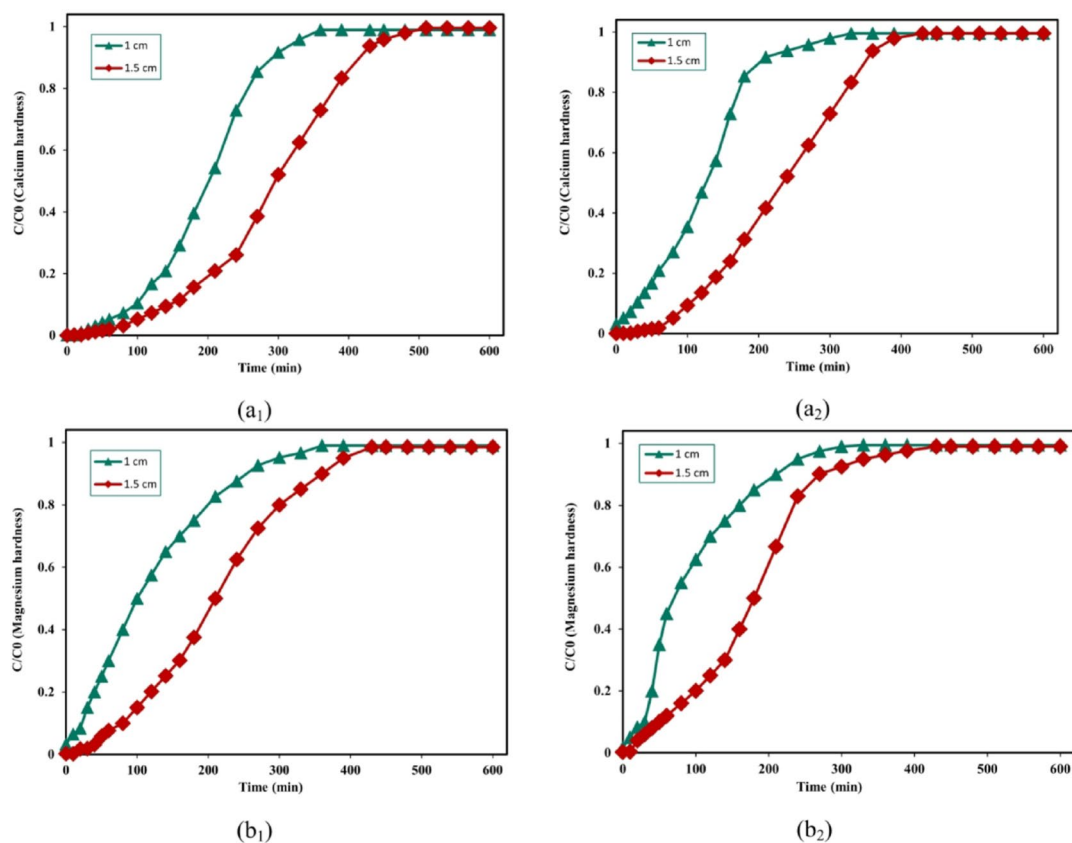


**Fig. 19.** The effect of column diameter and water flow in reducing (a) calcium hardness, and (b) magnesium hardness of drinking water by activated alumina ( $T = 25^{\circ}\text{C}$ ,  $\text{pH} = 7$ ), (a<sub>1</sub>, b<sub>1</sub>)  $Q = 10$  ml/min, (a<sub>2</sub>, b<sub>2</sub>)  $Q = 20$  ml/min.

drinking water. Modification with sulfuric acid increased the adsorption rate for both ions compared to the unmodified form; however, overall removal efficiency remained relatively low, indicating that further modification may be needed to improve performance.

For calcium hardness, breakthrough occurred at 80 min (1 cm) and 140 min (1.5 cm) at 10 ml/min, and 50 min and 80 min, respectively, at 20 ml/min. Bed saturation times were 500 min (1 cm) and 510 min (1.5 cm) at 10 ml/min, and 430 min and 480 min at 20 ml/min. The increase in adsorption rate is attributed to a greater number of active sites and larger surface area generated by the modification, which allowed more calcium ions to be adsorbed.

For magnesium hardness, breakthrough occurred at 30 min (1 cm) and 80 min (1.5 cm) at 10 ml/min, and 20 min and 50 min, respectively, at 20 ml/min. Bed saturation times were 480 min (1 cm) and 510 min (1.5 cm) at 10 ml/min, and 450 min and 480 min at 20 ml/min.

While the sulfuric acid modification enhanced adsorption capacity for both calcium and magnesium ions, the improvement was modest. Further research exploring alternative chemical modifiers may yield greater performance gains for hardness reduction in drinking water.

### Kinetic models of adsorption columns

Kinetic modeling was applied to describe the behavior of  $\text{Ca}^{2+}$  and  $\text{Mg}^{2+}$  removal in the continuous adsorption process using the Thomas, Adams–Bohart, and Yoon–Nelson models. Each model was fitted to experimental data to evaluate predictive accuracy and extract kinetic parameters, with results presented in Tables S1–S12 and Figs. 21, 22, 23, 24, 25, 26, 27, 28, 29, 30, 31 and 32.

To better justify the applicability of the kinetic models used in this study, the performance of the Thomas, Yoon–Nelson, and Adams–Bohart models was compared with findings reported in previous fixed-bed adsorption studies. The Thomas and Yoon–Nelson models showed consistently higher correlation coefficients ( $R^2 \approx 0.97$ – $0.99$ ) compared to the Adams–Bohart model, indicating superior predictive capability for the breakthrough behavior observed in this work. Similar trends have been reported for fixed-bed adsorption of hardness ions and other divalent metals, where the Thomas and Yoon–Nelson models were found to more accurately describe the overall mass transfer and saturation behavior of adsorption columns, particularly beyond the initial breakthrough region<sup>29,30</sup>. The relatively weaker performance of the Adams–Bohart model observed in this study is consistent with literature reports, as this model is primarily applicable to the initial portion of the breakthrough curve and does not adequately account for intraparticle diffusion and axial dispersion effects<sup>31</sup>. In contrast, the Thomas model incorporates adsorption capacity and mass transfer kinetics, while the Yoon–Nelson model offers a

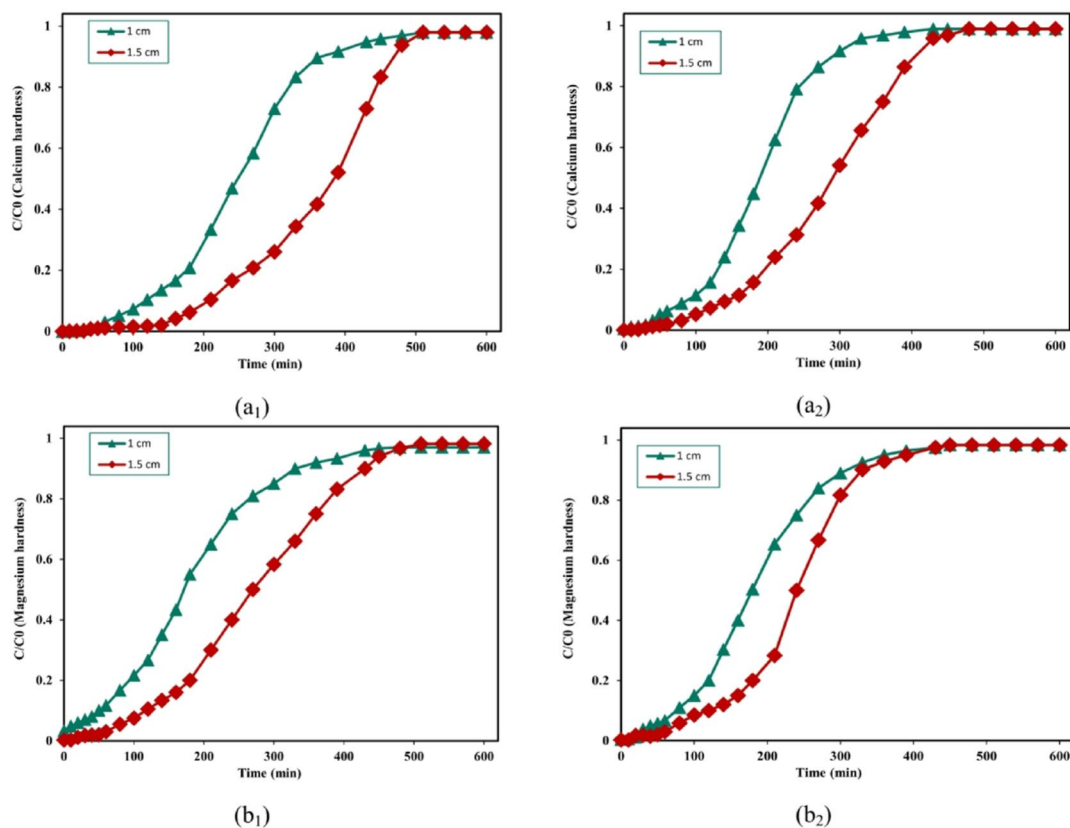


**Fig. 20.** The effect of column diameter and water flow on reducing (a) calcium hardness, and (b) magnesium hardness of drinking water by modified activated alumina ( $T = 25^\circ\text{C}$ ,  $\text{pH} = 7$ ), (a<sub>1</sub>, b<sub>1</sub>)  $Q = 10$  ml/min, (a<sub>2</sub>, b<sub>2</sub>)  $Q = 20$  ml/min.

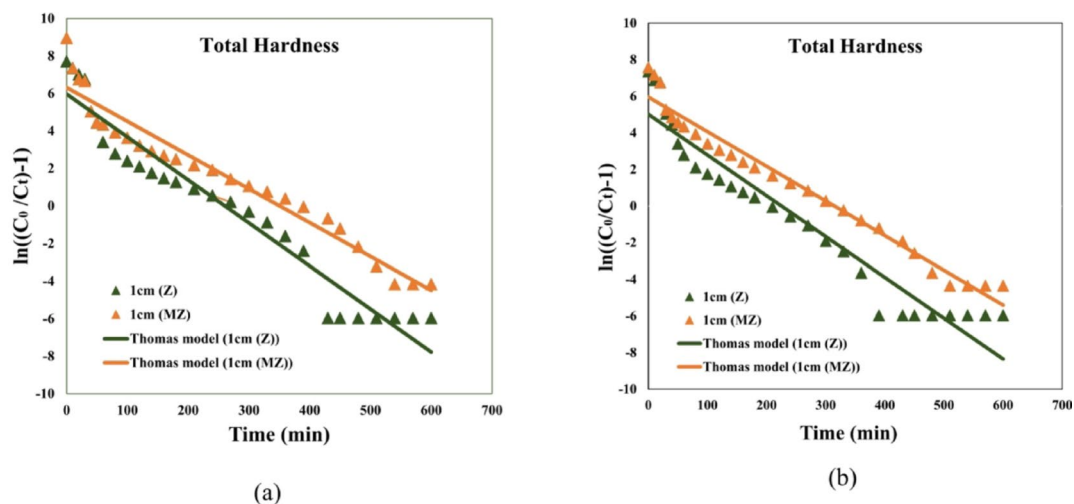


**Fig. 21.** Comparison of experimental and predicted fracture curves using the Thomas model for natural zeolite (Z) and modified zeolite (MZ) adsorbents in a 1 cm column at flow rate of (a)  $Q = 10$  mL/min, and (b)  $Q = 20$  ml/min for Total Hardness removal.

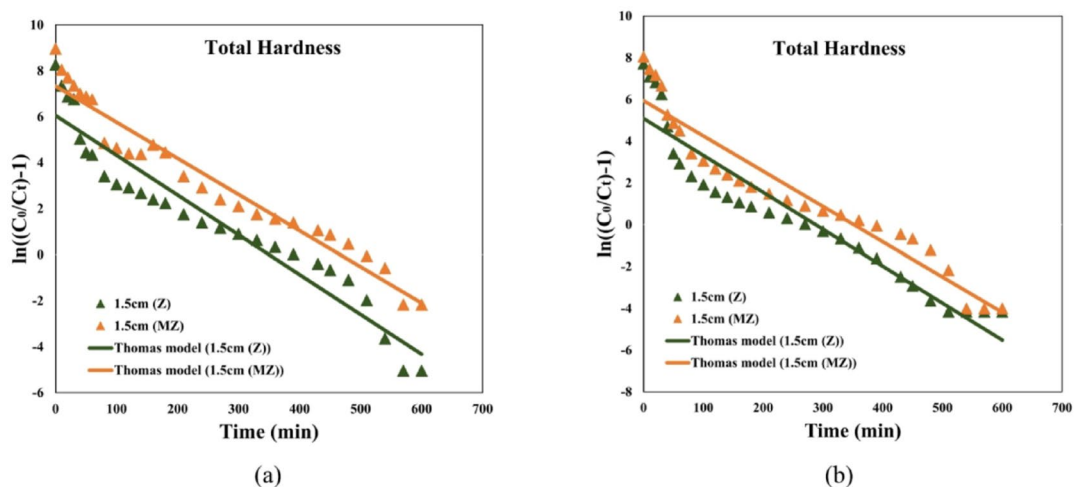


**Fig. 22.** Comparison of experimental and predicted fracture curves using the Thomas model for natural zeolite (Z) and modified zeolite (MZ) adsorbents in a 1.5 cm column at flow rate of (a)  $Q = 10$  mL/min, and (b)  $Q = 20$  ml/min for Total Hardness removal.

simplified yet robust description of breakthrough behavior without requiring detailed adsorbent properties. Recent studies have similarly highlighted the suitability of these models for evaluating continuous adsorption systems under practical operating conditions<sup>32,33</sup>. Therefore, the strong agreement between experimental data and the Thomas and Yoon–Nelson models in this study confirms their applicability for predicting hardness removal performance in modified ceramic adsorbent-based fixed-bed columns.

#### Thomas

The Thomas model, which assumes Langmuir-type adsorption and negligible axial dispersion, showed the best agreement with experimental data among the three models. High correlation coefficients ( $R^2 > 0.90$  in most cases) confirmed its suitability for simulating breakthrough behavior, especially for modified adsorbents.

For modified zeolite and modified activated alumina, the model fit was particularly strong across all flow rates and column diameters, with  $R^2$  values up to 0.98 (Tables S2 and S4). Predicted and experimental breakthrough curves aligned closely in Figs. 21, 22, 23 and 24 and similar trends for calcium and magnesium hardness are observed in Figures S1–S8.

For natural zeolite and activated alumina, good agreement was observed primarily in larger columns or at lower flow rates. Notably, model accuracy decreased slightly for magnesium removal at higher flow rates in 1 cm columns, possibly due to faster saturation and reduced contact time. Overall, the Thomas model effectively

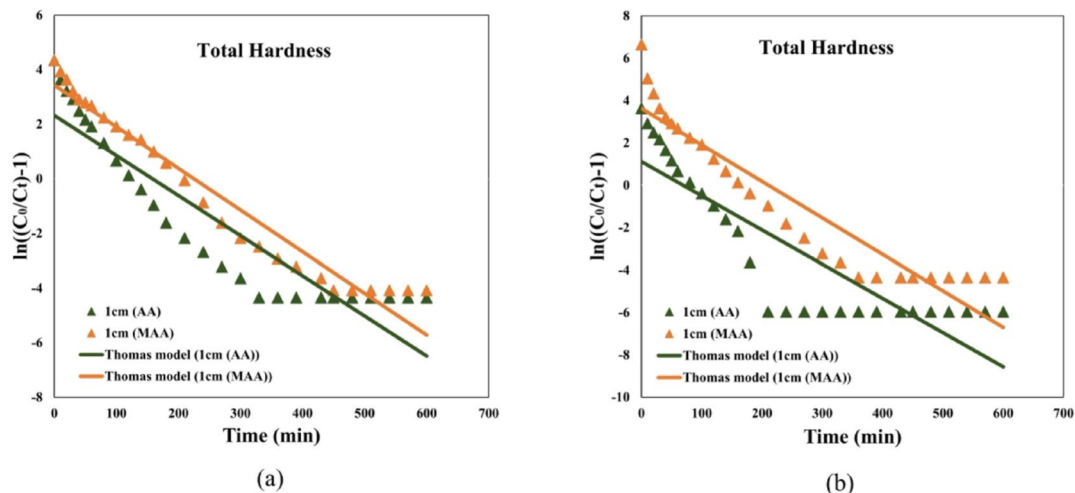


**Fig. 23.** Comparison of experimental and predicted fracture curves using the Thomas model for activated alumina (AA) and modified activated alumina (MAA) adsorbents in a 1 cm column at flow rate of (a)  $Q = 10$  mL/min, and (b)  $Q = 20$  mL/min for Total Hardness removal.

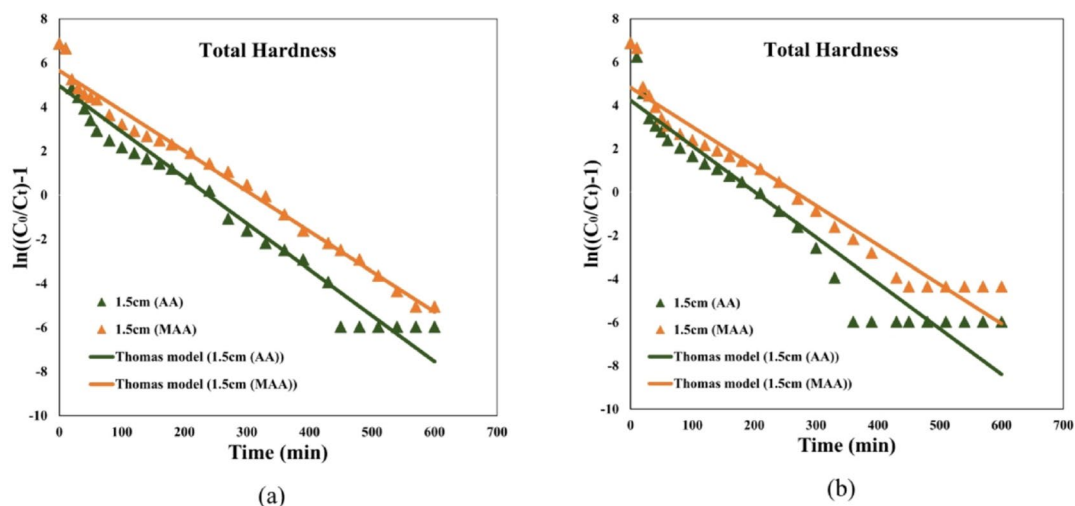


**Fig. 24.** Comparison of experimental and predicted fracture curves using the Thomas model for activated alumina (AA) and modified activated alumina (MAA) adsorbents in a 1.5 cm column at flow rate of (a)  $Q = 10$  mL/min, and (b)  $Q = 20$  mL/min for Total Hardness removal.

captured the ion exchange dynamics and is well-suited for column design and scaling in continuous hardness removal systems.

#### Adams-Bohart

The Adams–Bohart model focuses on the initial section of the breakthrough curve and assumes constant adsorption capacity along the bed. However, this model produced lower correlation coefficients ( $R^2 < 0.80$  in many cases) and did not accurately represent the experimental data for any of the adsorbents (Tables S5–S8).

Figures 25, 26, 27 and 28 show poor alignment between predicted and experimental curves, particularly at later time points, indicating the model's limitations under non-ideal flow conditions and multi-ion systems. These discrepancies suggest that the model's assumptions (e.g., linear driving force and uniform bed behavior) are insufficient for describing the full adsorption process in this study, with the breakthrough curves for calcium and magnesium hardness in Figures S9–S16 exhibiting similar deviations. Thus, while the Adams–Bohart model offers a quick estimation of initial performance, it lacks predictive power for complete breakthrough curve behavior in complex systems like water hardness removal.

#### Yoon-Nelson

The Yoon–Nelson model also provided a good fit to the data, particularly in estimating the time required for 50% adsorbate breakthrough ( $\tau$ ). High  $R^2$  values (often  $> 0.90$ ) were obtained across all adsorbents and conditions

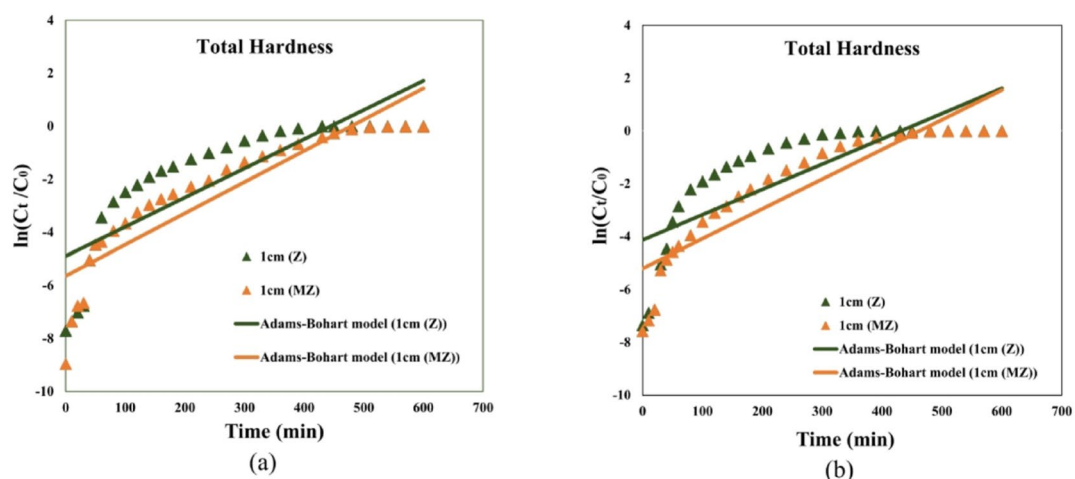


**Fig. 25.** Comparison of experimental and predicted fracture curves using the Adams-Bohart model for natural zeolite (Z) and modified zeolite (MZ) adsorbents in a 1 cm column at flow rate of (a)  $Q = 10$  mL/min, and (b)  $Q = 20$  ml/min for Total Hardness removal.

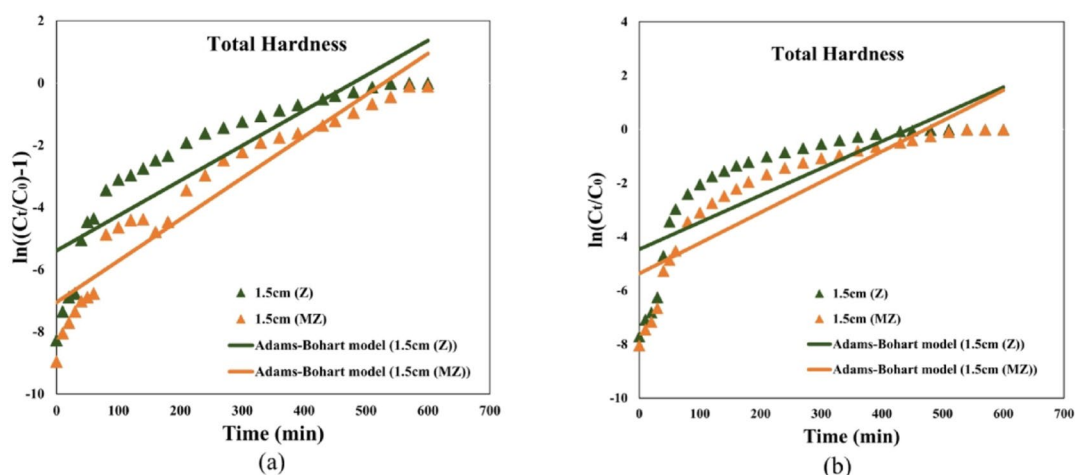


**Fig. 26.** Comparison of experimental and predicted fracture curves using the Adams-Bohart model for natural zeolite (Z) and modified zeolite (MZ) adsorbents in a 1.5 cm column at flow rate of (a)  $Q = 10$  mL/min, and (b)  $Q = 20$  ml/min for Total Hardness removal.

(Tables S9–S12), and the predicted breakthrough curves closely followed experimental trends (Figs. 29, 30, 31 and 32). Similar breakthrough trends for calcium and magnesium hardness are also evident in Figures S17–S24.

For modified zeolite,  $\tau$  values increased significantly compared to the natural form, indicating enhanced adsorption capacity and extended column life. For instance, total hardness  $\tau$  increased from 260 min to 467 min in the 1.5 cm column at 10 mL/min. A similar but smaller improvement was observed with modified activated alumina.

These results confirm that the Yoon–Nelson model is a reliable tool for predicting breakthrough behavior, particularly when simplified input parameters are desired. It also reinforces the role of adsorbent modification in prolonging effective operation time in fixed-bed systems.

#### Nonlinear model fitting results

In addition to the linearized kinetic models presented above, the nonlinear forms of the Thomas, Adams–Bohart, and Yoon–Nelson equations were applied to the total hardness adsorption data for all adsorbents (NZ, MZ, AA, and MAA) under the tested column diameters and flow rates. The complete nonlinear breakthrough curves are provided in the Supplementary Materials (Figures S25–S36), and the corresponding nonlinear model parameters are summarized in Tables S13–S15 for the Thomas, Adams–Bohart, and Yoon–Nelson models, respectively.

Overall, the nonlinear fitting results exhibited slightly higher coefficients of determination ( $R^2$ ) compared to the linearized forms, indicating a better representation of the experimental breakthrough curves. For example, in the case of the Thomas model,  $R^2$  values typically increased from  $\sim 0.94$  in the linear form to  $\sim 0.98$  in the

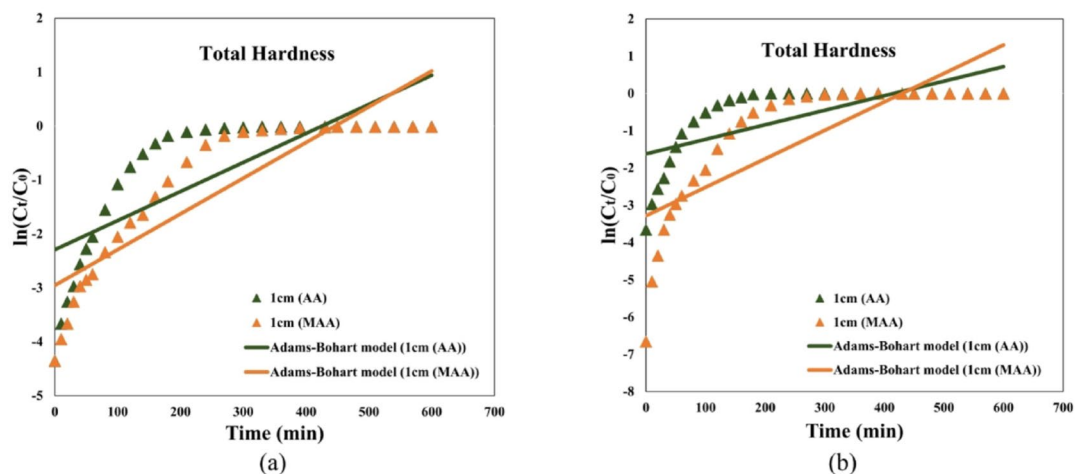


**Fig. 27.** Comparison of experimental and predicted fracture curves using the Adams-Bohart model for activated alumina (AA) and modified activated alumina (MAA) adsorbents in a 1 cm column at flow rate of (a)  $Q = 10$  mL/min, and (b)  $Q = 20$  mL/min for Total Hardness removal.

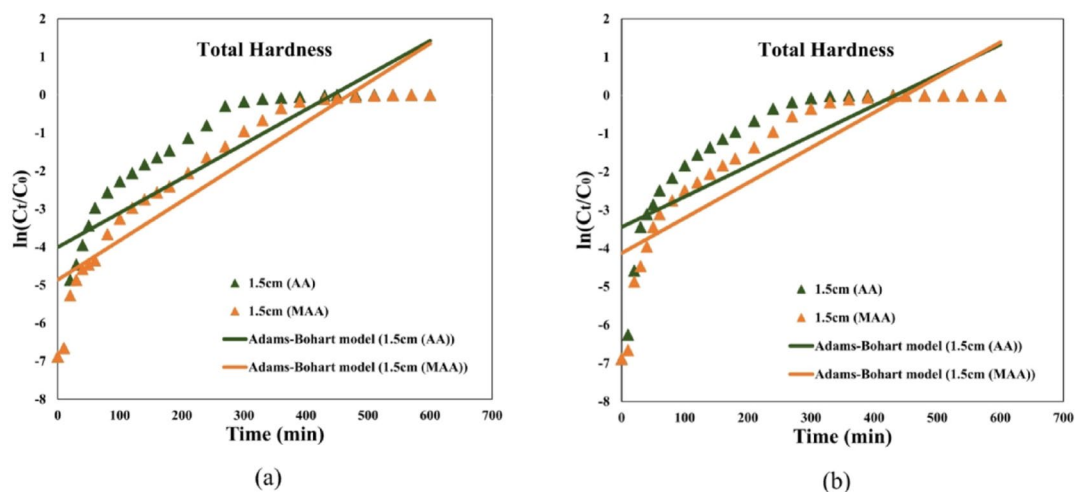


**Fig. 28.** Comparison of experimental and predicted fracture curves using the Adams-Bohart model for activated alumina (AA) and modified activated alumina (MAA) adsorbents in a 1.5 cm column at flow rate of (a)  $Q = 10$  mL/min, and (b)  $Q = 20$  mL/min for Total Hardness removal.

nonlinear form. Similarly, the Yoon-Nelson model showed notable improvement, with  $R^2$  values frequently exceeding 0.97. In contrast, the Adams-Bohart model remained the least accurate, despite minor increases in  $R^2$ . The improvement in nonlinear models is attributed to their direct fitting of the experimental data without transformation, which reduces potential bias introduced by linearization.

While nonlinear fitting offers more accurate parameter estimation, the linearized approach was also used in this study due to its simplicity, ease of graphical interpretation, and widespread application in column adsorption studies. Moreover, the linearized form facilitates straightforward comparison between different models under identical conditions, which is valuable when evaluating relative model performance. The results collectively suggest that for predictive purposes and detailed parameter analysis, the nonlinear form is preferable, whereas the linear form remains a practical and comparable tool for preliminary evaluation.

### Comparative study

Table 4 compares various studies on reducing the hardness of drinking water using different adsorbents and operational processes, including batch and fixed-bed methods. Most previous research utilized batch processes with adsorbents having small particle sizes, which increased the contact surface area between the water and the adsorbent. The most important parameters influencing the adsorption rate are the adsorbent's surface area and the contact duration between the adsorbents and water. The adsorbents used in previous research had high specific surface areas but were also expensive and economically unfavorable<sup>3,16,18,34</sup>.

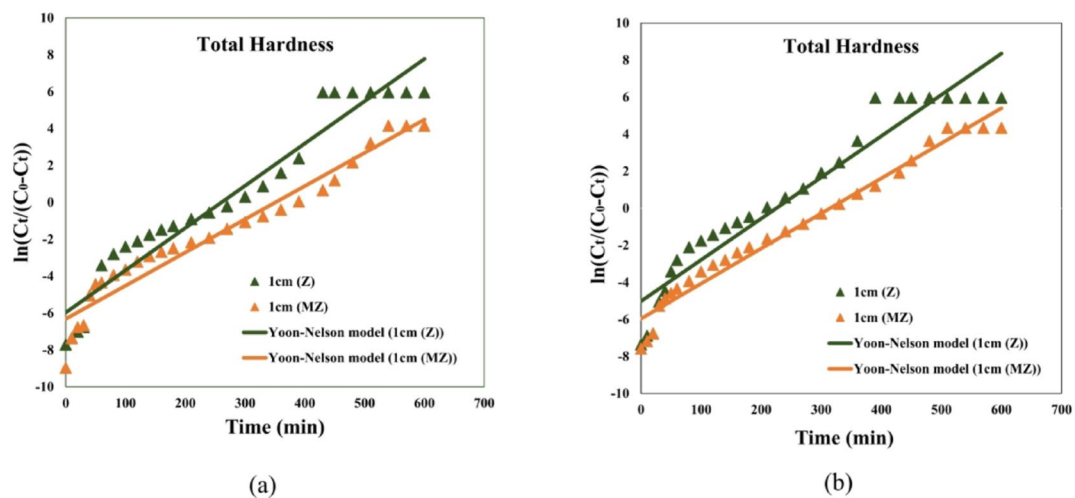


**Fig. 29.** Comparison of experimental and predicted fracture curves using the Yoon-Nelson model for natural zeolite (Z) and modified zeolite (MZ) adsorbents in a 1 cm column at flow rate of (a)  $Q = 10$  mL/min, and (b)  $Q = 20$  ml/min for Total Hardness removal.

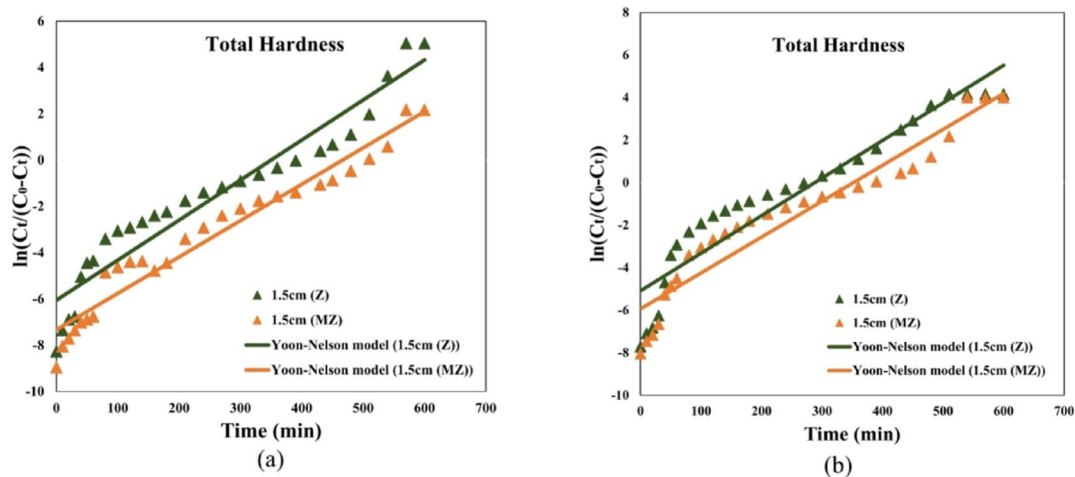


**Fig. 30.** Comparison of experimental and predicted fracture curves using the Yoon-Nelson model for natural zeolite (Z) and modified zeolite (MZ) adsorbents in a 1.5 cm column at flow rate of (a)  $Q = 10$  mL/min, and (b)  $Q = 20$  ml/min for Total Hardness removal.

In this study, low-cost adsorbents, specifically natural zeolite and activated alumina, were utilized. A new design of fixed-bed adsorption columns was introduced, which greatly improved the removal efficiency. This improvement was attributed to the porous structure of natural zeolite, which, despite its relatively low surface area, still achieved high removal efficiency. Additionally, the increased contact duration between water and adsorbents in the fixed-bed column with low-cost adsorbents further improved the removal efficiency. The removal efficiency was estimated at more than 99.23% for natural zeolite and 98.71% for activated alumina. Table 5 summarizes the removal efficiency results for all test conditions. According to these results, the adsorbents can be used on an industrial scale due to their low cost and high efficiency.

The materials used in this research are abundantly available and very inexpensive compared to typical commercial water-softening media. Natural clinoptilolite zeolite, for instance, is mined at low cost, on the order of only USD 30–70 per ton ( $\approx 0.03$ – $0.07$  USD/kg) for granular grades<sup>35</sup>. Activated alumina, purchased locally from industrial suppliers in Iran, is priced around 0.35–0.5 USD/kg, depending on purity and granule size. Even with added surface modification steps, the cost remains far below that of standard market adsorbents. Granular activated carbon (GAC), one of the most common commercial adsorbents, usually sells for approximately 2–3 USD per kg<sup>36</sup>. Likewise, commercial ion exchange resins used for hardness removal are even more expensive, typically costing between 4 and 10 USD/kg in the Iranian market.

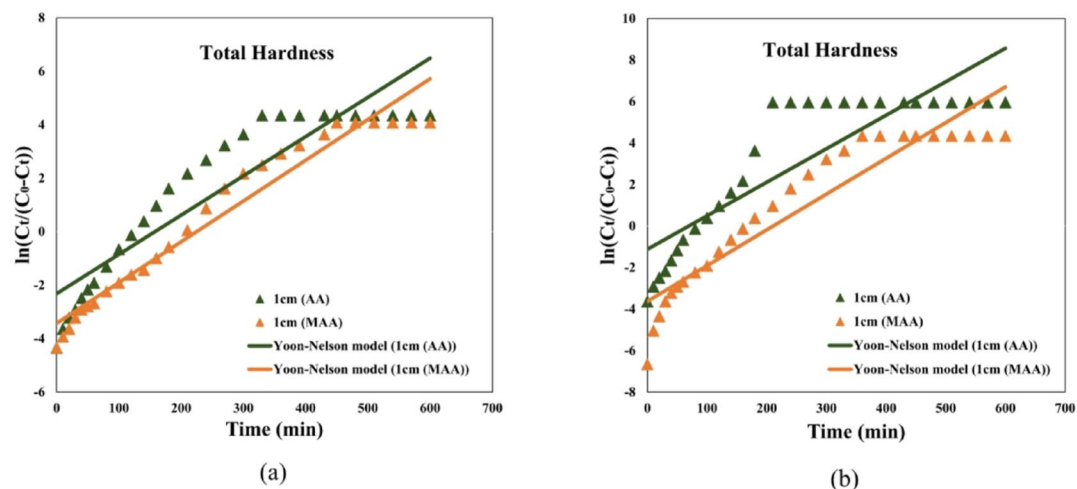


**Fig. 31.** Comparison of experimental and predicted fracture curves using the Yoon-Nelson model for activated alumina (AA) and modified activated alumina (MAA) adsorbents in a 1 cm column at flow rate of (a)  $Q = 10$  mL/min, and (b)  $Q = 20$  mL/min for Total Hardness removal.

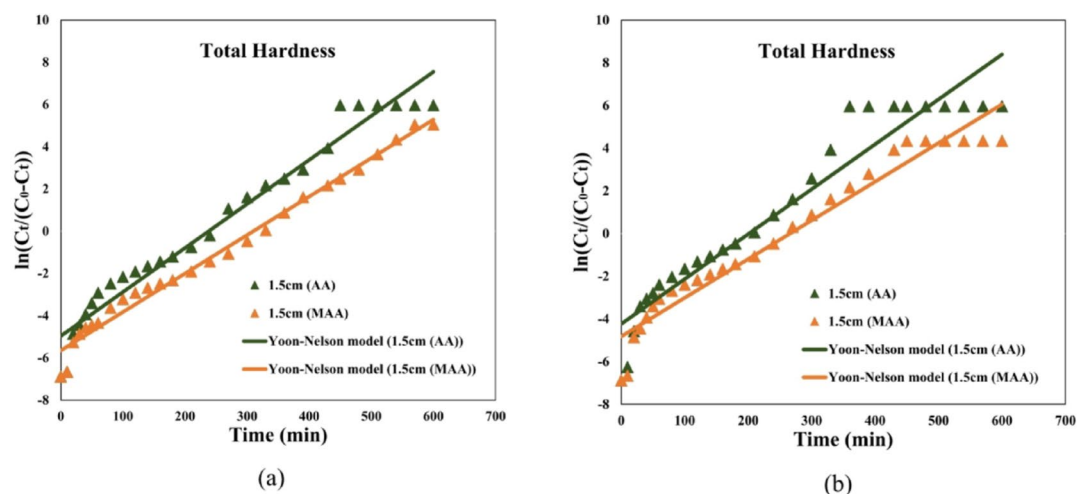


**Fig. 32.** Comparison of experimental and predicted fracture curves using the Yoon-Nelson model for activated alumina (AA) and modified activated alumina (MAA) adsorbents in a 1.5 cm column at flow rate of (a)  $Q = 10$  mL/min, and (b)  $Q = 20$  mL/min for Total Hardness removal.

| No. | Adsorbent  | Removal efficiency (%) | Ref.          |
|-----|--|------------------------|---------------|
| 1   | Natural Zeolite & SSF  | 66                     | 16            |
| 2   | Coconut Shell Activated Carbon (CSAC)                          | 55                     | 34            |
| 3   | Sodalite from Muscovite (M.SD)                                 | 90.5                   | 18            |
| 4   | Natural Zeolite & Activated Alumina & Activated Carbon (batch) | 93.07, 30.76, 56.92    | 3             |
| 5   | Natural Zeolite & Modified Natural Zeolite (fixed - bed)       | 96, 99.23              | Current study |
| 6   | Activated Alumina & Modified Activated Alumina (fixed-bed)     | 95, 98.71              | Current study |

**Table 4.** Removal efficiency of reducing of water hardness with different adsorbent.

Moreover, the modification processes used to enhance the zeolite and activated alumina, simple treatments involving inexpensive chemicals such as  $\text{NaNO}_3$  and  $\text{H}_2\text{SO}_4$ , are straightforward, scalable, and add only minimal cost. Unlike high-tech synthesis methods or costly activation procedures, this approach relies on basic, widely available reagents such as sodium salts and mineral acids. As a result, the modified adsorbents retain their low-cost nature even after treatment. Previous studies have also reported that natural clay- or zeolite-based sorbents

|                            | Z (cm) | Q (ml/min) | Total hardness | Calcium hardness | Magnesium Hardness |
|----------------------------|--------|------------|----------------|------------------|--------------------|
| Natural Zeolite            | 1      | 10         | 96.79          | 96.25            | 97                 |
|                            | 1      | 20         | 94.23          | 93.75            | 94                 |
|                            | 1.5    | 10         | 98.71          | 98.2             | 98.25              |
|                            | 1.5    | 20         | 94.48          | 94.25            | 94                 |
| Modified Zeolite           | 1      | 10         | 98.71          | 98.12            | 98.36              |
|                            | 1      | 20         | 96.79          | 97               | 97.5               |
|                            | 1.5    | 10         | 99.23          | 99.37            | 99.17              |
|                            | 1.5    | 20         | 98.91          | 98.12            | 98.3               |
| Activated Alumina          | 1      | 10         | 95             | 94.8             | 94                 |
|                            | 1      | 20         | 92.3           | 92.7             | 91.67              |
|                            | 1.5    | 10         | 96.79          | 96.87            | 96.83              |
|                            | 1.5    | 20         | 94             | 94.81            | 94                 |
| Modified Activated Alumina | 1      | 10         | 97.43          | 96.87            | 96.7               |
|                            | 1      | 20         | 94.87          | 94.79            | 94.25              |
|                            | 1.5    | 10         | 98.71          | 98.64            | 98                 |
|                            | 1.5    | 20         | 95.51          | 96.87            | 96.23              |

**Table 5.** Removal efficiency results (%) for different adsorbents under various conditions.

can be effectively regenerated or modified using simple sodium solutions in a cost-efficient manner, thereby preserving their economic advantages<sup>35</sup>. Collectively, these factors make the modified zeolite and activated alumina a highly cost-effective alternative to conventional adsorbents for water softening. The process achieves comparable hardness removal performance at a fraction of the material cost associated with commercial ion-exchange resins or activated carbon, an especially important consideration for large-scale or resource-limited water treatment applications.

## Conclusions

In this research, natural zeolite adsorbents and activated alumina, both in their modified forms with sodium nitrate and sulfuric acid, were used to investigate the adsorption of hardness ions (calcium and magnesium ions) in fixed-bed columns with diameters of 1 and 1.5 cm and flow rates of 10 ml/min and 20 ml/min. The experimental results were then compared with various kinetic models for adsorption column performance.

The findings of this study reveal that the adsorption rate of hardness ions by the ceramic adsorbents (natural zeolite and activated alumina) increased with an increase in column diameter, while it decreased with higher flow rates. Based on the tests conducted, the most favorable condition and the best adsorbent for achieving the desired results were found to be using natural zeolite in a 1.5 cm column at a flow rate of 10 ml/min. The observed time intervals for breakthrough were 120 min, 120 min, and 100 min for total hardness, calcium hardness, and magnesium hardness, respectively. Furthermore, the saturated time intervals for total hardness, calcium hardness, and magnesium hardness were 570 min, 540 min, and 570 min, respectively.

In order to enhance the adsorbent performance, the use of NaNO<sub>3</sub> and H<sub>2</sub>SO<sub>4</sub> modifiers for natural zeolite and activated alumina, respectively, was employed. The modification of natural zeolite led to significantly longer breakthrough time intervals in the best test condition, reaching 240 min, 180 min, and 450 min for total hardness, calcium hardness, and magnesium hardness, respectively, compared to the unmodified state. This improvement was attributed to the increase in adsorption capacity due to ion exchange with sodium nitrate. Similarly, the saturated time intervals also increased in this case for total hardness, calcium hardness, and magnesium hardness, taking 600 min for the bed to reach saturation due to the enhanced adsorption capacity of zeolite.

The kinetics of the adsorption column for total hardness, calcium hardness, and magnesium hardness on the adsorbents were studied using three models: Thomas, Adams–Bohart, and Yoon–Nelson. Upon analyzing the correlation coefficients (R<sup>2</sup>), the laboratory data exhibited the best agreement with the Thomas and Yoon–Nelson kinetic models, both in their linear and non-linear forms. Incorporating non-linear modeling improved the fitting accuracy for all models, with R<sup>2</sup> values for Thomas and Yoon–Nelson increasing up to 0.98 for total hardness, confirming their suitability for describing the adsorption process. Although the Adams–Bohart model also showed slightly better performance in the non-linear form, its overall predictive accuracy remained lower. The best conditions for total hardness, calcium hardness, and magnesium hardness exhibited outstanding removal efficiencies of 99.23%, 99.37%, and 99.17%, respectively, highlighting the effectiveness of the utilized adsorbents in reducing hardness ions from the drinking water samples. The comparative evaluation of kinetic models further demonstrated that the Thomas and Yoon–Nelson models provide a more reliable description of the adsorption behavior in the fixed-bed columns compared to the Adams–Bohart model, which was limited to the initial breakthrough region. This observation is consistent with previous studies on continuous adsorption systems and confirms the suitability of these models for predicting the performance of modified ceramic adsorbents under practical operating conditions.

In conclusion, this study highlights the effectiveness of natural zeolite and activated alumina as adsorbents for the removal of hardness ions from drinking water. The modification of adsorbents with NaNO<sub>3</sub> and H<sub>2</sub>SO<sub>4</sub>

further enhanced their adsorption capacities, making them even more suitable for water treatment applications. The application of kinetic models provided valuable insights into the behavior of the adsorption process in fixed-bed columns, aiding in the optimization of operating conditions for efficient hardness removal. Overall, this research contributes to the advancement of water treatment technologies and provides valuable information for designing effective adsorption systems for the removal of hardness ions from drinking water sources.

### Data availability

The datasets used and analyzed in the study are available from the corresponding author (m.abbasi@pgu.ac.ir) upon reasonable request.

Received: 22 May 2025; Accepted: 2 February 2026

Published online: 14 February 2026

### References

- Moreira, N. & Bondelind, M. Safe drinking water and waterborne outbreaks. *J. Water Health*. **15** (1), 83–96 (2017).
- Miller, J. D. et al. Self-reported anticipated harm from drinking water across 141 countries. *Nat. Commun.* **15** (1), 7320 (2024).
- Ghanbarizadeh, P. et al. Performance enhancement of specific adsorbents for hardness reduction of drinking water and groundwater. *Water* **14** (17), 2749 (2022).
- Akram, S. & Rehman, F. Hardness in drinking-water, its sources, its effects on humans and its household treatment. *J. Chem. Appl.* **4** (1), 1–4 (2018).
- Świątlik, J. et al. Corrosion in drinking water pipes: the importance of green rusts. *Water Res.* **46** (1), 1–10 (2012).
- Amin, M. T., Alazba, A. A. & Manzoor, U. A review of removal of pollutants from water/wastewater using different types of nanomaterials. *Adv. Mater. Sci. Eng.* **2014**, 1–24 (2014).
- Henthorne, L. & Boysen, B. State-of-the-art of reverse osmosis desalination pretreatment. *Desalination* **356**, 129–139 (2015).
- Ping, Q. et al. Long-term investigation of fouling of cation and anion exchange membranes in microbial desalination cells. *Desalination* **325**, 48–55 (2013).
- Campanile, A. et al. Zeolite-based monoliths for water softening by ion exchange/precipitation process. *Sci. Rep.* **12** (1), 3686 (2022).
- Goud, R. V. et al. Comparison studies on adsorbants for removal of hardness from water by using newly prepared zeolite. *Int. J. Adv. Pharm. Biology Chem.* **4**, 342–354 (2015).
- Pinto, P. X. et al. Bench-scale and pilot-scale treatment technologies for the removal of total dissolved solids from coal mine water: a review. *Mine Water Environ.* **35** (1), 94–112 (2016).
- Hamidpour, M. et al. Sorption hysteresis of Cd (II) and Pb (II) on natural zeolite and bentonite. *J. Hazard. Mater.* **181** (1–3), 686–691 (2010).
- Badalians Gholikandi, G. et al. Natural zeolites application as sustainable adsorbent for heavy metals removal from drinking water. *Iran. J. Toxicol.* **3** (3), 302–310 (2010).
- Yusof, A. M. et al. Removal of Ca<sup>2+</sup> and Zn<sup>2+</sup> from aqueous solutions by zeolites nap and KP. *Environ. Technol.* **31** (1), 41–46 (2010).
- Sepehr, M. N. et al. Removal of hardness agents, calcium and magnesium, by natural and alkaline modified pumice stones in single and binary systems. *Appl. Surf. Sci.* **274**, 295–305 (2013).
- Abdolahnejad, A., Ebrahimi, A. & Jafari, N. Application of Iranian natural zeolite and blast furnace slag as slow sand filters media for water softening. *Int. J. Environ. Health Eng.* **3** (1), 26 (2014).
- Kumari, U., Behera, S. K. & Meikap, B. A novel acid modified alumina adsorbent with enhanced defluoridation property: kinetics, isotherm study and applicability on industrial wastewater. *J. Hazard. Mater.* **365**, 868–882 (2019).
- Salam, M. A. et al. Effective decontamination of Ca<sup>2+</sup> and Mg<sup>2+</sup> hardness from groundwater using innovative Muscovite based sodalite in batch and fixed-bed column studies; dynamic and equilibrium studies. *J. Contam. Hydrol.* **241**, 103817 (2021).
- Kaewmee, P., Hungwe, D. & Takahashi, F. Adsorptive reduction of water hardness by a highly porous and regenerative geopolymer fabricated from coal fly Ash waste with low-temperature calcination. *Environ. Sci. Pollut. Res.* **28** (39), 54594–54607 (2021).
- Mubarak, M. F. et al. Adsorption of heavy metals and hardness ions from groundwater onto modified zeolite: batch and column studies. *Alexandria Eng. J.* **61** (6), 4189–4207 (2022).
- Ali, A. et al. Synchronous removal of Ca<sup>2+</sup>, Cd<sup>2+</sup>, Zn<sup>2+</sup>, and NO<sub>3</sub><sup>-</sup> from water using magnetic Biochar-Based bioceramsite reactor: an advanced technique for water remediation. *Earth Syst. Environ. Volume*. **8**, 895–910 (2024).
- Rice, E. W., Bridgewater, L. & Association, A. P. H. *Standard Methods for the Examination of Water and Wastewater* Vol. 10 (American public health association Washington, DC, 2012).
- Thomas, H. C. Chromatography: a problem in kinetics. *Ann. N. Y. Acad. Sci.* **49** (2), 161–182 (1948).
- Bakhta, S. et al. Successful removal of fluoride from aqueous environment using Al(OH)<sub>3</sub>@AC: column studies and breakthrough curve modeling. *RSC Adv.* **14** (1), 1–14 (2024).
- Lodeiro, P., Herrero, R. & de Vicente, M. S. The use of protonated sargassum muticum as biosorbent for cadmium removal in a fixed-bed column. *J. Hazard. Mater.* **137** (1), 244–253 (2006).
- Fu, H. et al. Ammonium removal using a calcined natural zeolite modified with sodium nitrate. *J. Hazard. Mater.* **393**, 122481 (2020).
- Dehghan, P. et al. Application of sodium Dodecyl sulfate modified zeolite for effective adsorption of kinetic hydrate inhibitor compounds from aqueous solution. *J. Mol. Liq.* **402**, 124734 (2024).
- Bagheri, H. et al. Experimental evaluation of Farashband gas refinery wastewater treatment through activated carbon and natural zeolite adsorption process. *Desalination Water Treat.* **225**, 190–202 (2021).
- Omitola, O. B. et al. Adams-Bohart, Yoon-Nelson, and Thomas modeling of the fix-bed continuous column adsorption of amoxicillin onto silver nanoparticle-maize leaf composite. *Appl. Water Sci.* **12** (5), 94 (2022).
- Recepoglu, Y. K. et al. Packed bed column dynamic study for Boron removal from geothermal Brine by a chelating fiber and breakthrough curve analysis by using mathematical models. *Desalination* **437**, 1–6 (2018).
- Jiang, S. et al. Continuous adsorption removal of organic pollutants from wastewater in a UiO-66 fixed bed column. *J. Environ. Chem. Eng.* **12** (2), 111951 (2024).
- Zahakifar, F. & Khanramaki, F. Continuous removal of thorium from aqueous solution using functionalized graphene oxide: study of adsorption kinetics in batch system and fixed bed column. *Sci. Rep.* **14** (1), 14888 (2024).
- Recepoglu, Y. K. & Yüksel, A. Cross-linked phosphorylated cellulose as a potential sorbent for lithium extraction from water: dynamic column studies and modeling. *ACS Omega*. **7** (43), 38957–38968 (2022).
- Rolence, C., Machunda, R. & Njau, K. Water hardness removal by coconut shell activated carbon. *East. Asian Sci. Technol. Soc. Int. J.* **2** (5), 97–102 (2014).
- Eberle, S., Börnick, H. & Stolte, S. Granular natural zeolites: cost-effective adsorbents for the removal of ammonium from drinking water. *Water* **14** (6), 939 (2022).

36. León, M. et al. Design, cost Estimation and sensitivity analysis for a production process of activated carbon from waste nutshells by physical activation. *Processes* **8** (8), 945 (2020).

### Acknowledgements

The authors acknowledge the Bushehr Province Water and Wastewater Company, Iran, for their financial support.

### Author contributions

Elnaz Danesh: Conceptualization, Data curation, Formal analysis, Investigation, Methodology, Writing – original draft, Writing – review and editing. Mohsen Abbasi: Conceptualization, Funding acquisition, Methodology, Project administration, Resources, Supervision, Writing – review and editing. MohammadMahdi Noroozi: Data curation, Formal analysis, Writing – original draft, Writing – review and editing. Masoud Mofarehi: Resources, Supervision, Writing – review and editing. Ali Izadbakhsh: Supervision. Mohammad Akrami: Resources, Writing – review and editing.

### Funding

This research did not receive any specific grant from funding agencies in the public, commercial, or not for profit sectors.

### Declarations

### Competing interests

The authors declare no competing interests.

### Declaration of generative AI and AI-assisted technologies in the writing process

During the preparation of this work the authors used ChatGPT-4o in order to improve readability of the text. After using this tool/service, the authors reviewed and edited the content as needed and takes full responsibility for the content of the published article.

### Additional information

**Supplementary Information** The online version contains supplementary material available at <https://doi.org/10.1038/s41598-026-38953-2>.

**Correspondence** and requests for materials should be addressed to M.A.

**Reprints and permissions information** is available at [www.nature.com/reprints](http://www.nature.com/reprints).

**Publisher's note** Springer Nature remains neutral with regard to jurisdictional claims in published maps and institutional affiliations.

**Open Access** This article is licensed under a Creative Commons Attribution-NonCommercial-NoDerivatives 4.0 International License, which permits any non-commercial use, sharing, distribution and reproduction in any medium or format, as long as you give appropriate credit to the original author(s) and the source, provide a link to the Creative Commons licence, and indicate if you modified the licensed material. You do not have permission under this licence to share adapted material derived from this article or parts of it. The images or other third party material in this article are included in the article's Creative Commons licence, unless indicated otherwise in a credit line to the material. If material is not included in the article's Creative Commons licence and your intended use is not permitted by statutory regulation or exceeds the permitted use, you will need to obtain permission directly from the copyright holder. To view a copy of this licence, visit <http://creativecommons.org/licenses/by-nc-nd/4.0/>.

© The Author(s) 2026